Materials Today Bio 13 (2022) 100204

Contents lists available at ScienceDirect

Materials Today Bio

journal homepage: www.journals.elsevier.com/materials-today-bio

Cinnamomum verum-derived bioactives-functionalized gold nanoparticles for prevention of obesity through gut microbiota reshaping

Vivek K. Sharma [1], Prateeksha [1], Sateesh C. Gupta, Brahma N. Singh [*], Chandana V. Rao, Saroj K. Barik [**]

Pharmacology Division, CSIR-National Botanical Research Institute, Lucknow, 226001, India

ARTICLE INFO

Keywords:
Gold nanoparticles
Cinnamomum verum
Polyphenols
Obesity
Gut microbiota
Bile acids

ABSTRACT

Existing drugs have limited success in managing obesity in human due to their low efficacy and severe side-effects. Surface-modified gold nanoparticles have now received considerable attention of researchers for efficient biomedical applications owing to their superior uptake by cells, biocompatibility, hydrophilicity and non-immunogenicity. Here we prepared *Cinnamomum verum* derived bioactives-functionalized gold nanoparticles (Au@P-NPs) and assessed their impact on obesity and related immune-metabolic complications in high-fat diet (HFD)-induced obese mice using metabolic experiments along with 16S RNA gene-based gut microbial profiling and faecal microbiota transplantation (FMT). Au@P-NPs treatment prevented weight gain, decreased fat deposition, reduced metabolic inflammation and endotoxaemia in HFD-fed mice. Au@P-NPs-treated group exhibited better glucose tolerance and insulin sensitivity than HFD-fed control mice, and got completely protected against hepatic steatosis. These impacts were related to increased energy expenditure and enhanced *Ucp1* expression in the brown adipose tissues of Au@P-NPs-administered animals, which strongly linked with the mRNA expression of the membrane bile acid receptor TGR5. Treatment of HFD-fed animals with Au@P-NPs altered plasma bile acid profile, and increased *Akkermansia muciniphila* and decreased *Lactobacillus* populations in the faeces. Au@P-NPs-treated animals revealed altered plasma bile acid profile, and increased *Akkermansia muciniphila* and decreased *Lactobacillus* populations in the faeces. FMT experiments showed lesser weight gain and greater energy expenditure in the mice fed with faecal suspension from Au@P-NPs-treated animals than that from HFD-fed mice. These results clearly establish that gold nanoparticles functionalized with bioactive compounds of *C. verum* have high potential to be an anti-obesity drug.

1. Introduction

Obesity along with related metabolic complications is now a major health concern worldwide and has become an economic and social burden [1]. It is predicted that at least one billion world population will be obese by 2030 [2]. Severe obesity contributes to the progression of a variety of disorders, including insulin resistance, type-2 diabetes, dyslipidemia, atherosclerosis and cancer [3,4]. Growing evidence has demonstrated that genetic and environmental factors are major causes of dysregulation of the balance between energy intake and expenditure which result in the storage of excess fat in adipose tissues [5]. Despite considerable efforts by the scientific community and pharmaceutical industry to discover new anti-obesity agents, obesity remains a major health challenge globally. The commercialized drugs viz., lorcaserin, topiramate and orlistat have very limited effect that reduce only 3–10% of the body weight. As such, most of them have been withdrawn from the market due to their severe side effects such as diarrhoea, headache, faecal incontinence and dyspepsia [6].

Recently, a growing body of research revealed a fundamental link between gut microbiota dysbiosis and obesity development, chiefly through regulation of nutrient acquisition, energy expenditure and fat deposition [7–11]. In most cases, obese people exhibit altered gut microbial diversity [12] and bacterial richness [9]. 16S rRNA gene-based sequence revealed a high ratio of the key phyla Firmicutes to Bacteroidetes (F/B), which could be linked with weight gain and metabolic dysfunctions [13]. Recent works have revealed that germ-free (GF) mice

* Corresponding author.
** Corresponding author.
E-mail addresses: bn.singh@nbri.res.in (B.N. Singh), sarojkbarik@gmail.com (S.K. Barik).
[1] Contributed equally.

https://doi.org/10.1016/j.mtbio.2022.100204
Received 11 August 2021; Received in revised form 11 January 2022; Accepted 11 January 2022
Available online 19 January 2022

gain less body weight despite a high fat-diet intake than that of non-GF mice [14]. Moreover, after transplantation of gut microbiota in GF receivers using faecal re-suspension from doner obese mice, the obesity characteristics appeared in the receiver mice [15]. These accumulating evidences have suggested that gut microbiota play a major role in the regulation of obesity.

Bile acids are synthesized from cholesterol in the liver and are required for the absorption of lipids and fatsoluble vitamins [16]. Gut microbiota convert primary bile acids to secondary bile acids through various reactions, namely deconjugation, dehydrogenation, and dihydroxylation [17]. In addition, bile acids stimulate Takeda G-protein coupled receptor 5 (TGR5) that enhance brown adipose tissue (BAT) activation, white adipose tissue (WAT) browning, and energy expenditure through UCP1 signalling [18]. Thus, TGR5 and UCP1 signalling modulation by bile acids through gut microbiota reshaping can provide a promising strategy for the prevention and treatment of obesity and related disorders.

Dietary polyphenols of *Cinnamomum verum* J. Presl (family: Lauraceae) have the potential to reduce weight gain, inflammation and insulin resistance, producing potent anti-obesity effects via gut microbiota remodeling [19–21]. However, these effects proven through preclinical and clinical studies are inadequate because of the limited bioavailability of therapeutically active phytochemicals of *C. verum* in gut environment [22]. *Ayurveda*, an ancient Indian medicine system that dates back to 5000 B.C., uses phytochemicals-coated gold nanoparticles (AuNPs) also known as *Swarna bhasma* for enhancing bioavailability of phytochemicals to treat bronchial asthma, rheumatoid arthritis, diabetes mellitus, liver, and indigestion [21,23]. A similar approach has also been followed by Chinese and Egyptian civilization since 2500 B.C [23,24]. The surface-functionalized NPs, particularly AuNPs are increasingly being used for drug delivery and diverse biomedical applications in recent years due to their excellent bio-compatibility, hydrophilicity, non-immunogenicity properties, and superior therapeutic benefits [25–34]. Plant metabolites-coated AuNPs could reduce fat accumulation in 3T3-L1 adipocyte cells through adipogenesis inhibition, an essential process responsible for forming fat cells [35]. On the other hand, the underlying mechanisms of these effects of AuNPs have not yet been fully elucidated. Earlier studies have demonstrated the role of various plant polyphenols in BAT activation through gut microbiota reshaping that leads to enhanced WAT browning and energy expenditure [36–41]. This encouraged us to study if surface-functionalized AuNPs exert anti-obesity effect via gut microbiota remodeling. Thus, the objective of this investigation was to develop *C. verum* derived bioactives-functionalized Au-NPs (Au@P-NPs) and elucidate their mechanisms underlying the beneficial effects on diet-induced obesity and related immunometabolic complications. The results of our investigation clearly reveal the possible mechanism of actions by which biocompatible Au@P-NPs increase BAT activation and WAT browning and might offer Au@P-NP as an anti-obesity drug.

2. Materials and methods

2.1. Materials

We procured chloroauric acid ($HAuCl_4$) and sodium citrate from HiMedia Laboratories Pvt., Ltd. (Maharashtra, India). We bought polyvinylpropylene from Sigma-Aldrich, USA. *C. verum* bark was procured from local market. We received ELISA kits of IL-1β, IL-6, INF-γ, VEGF, and RANTES from R & D Systems, Canada. CD36, FAS, FABP4, PPARγ, and ACC antibodies were procured from Thermo Fisher Scientific and Abcam.

2.2. Synthesis and characterization of NPs

We prepared citrate-capped gold nanoparticles (Au-NPs) and *C. verum* derived bioactives-functionalized Au-NPs (Au@P-NPs) in our laboratory. The detailed methods of their synthesis has been provided in the Supplementary Information section. We characterized the synthesized NPs by UV–vis spectrophotometer (UV201, Thermo Fisher Scientific, USA). A drop of diluted NPs was deposited on a copper grid and left to dry for 12 h at room temperature. We observed the NPs with a transmission electron microscope (TEM) at 200 kV (JEOL JEM-2100, Japan). The average sizes and zeta potentials of NPs were measured by a Zetasizer MAL1010294 (Malvern, UK). Fourier-transmission infrared spectroscopy (FTIR) was used to examine the functionalization of phytochemicals of *C. verum* on the surface of NPs (PerkinElmer Life and Analytical Sciences, CT, USA).

2.3. Animals

Eight-weeks-old male Swiss mice were obtained from CSIR-Central Drug Research Institute, India and independently housed in a controlled room (22 ± 1 °C temperature; 45–55% relative humidity) under 12 h daylight and 12 h without light with free access to sterile food pellets and water ad libitum in the animal house. The experiments were performed in accordance with the guidelines of the Committee for the Purpose of Supervision of Experiments on Animals (CPCSEA), India, as approved and promoted by the Institutional Animal Ethics Committee (Registration No. 1732/GO/Re/S/13/CPCSEA). After 2 weeks of acclimatization on a chow diet (CD; Bajaj Instrument Works, Ghaziabad), animals were arbitrarily distributed into 4 groups (n = 6) and fed on CD or a high-fat diet (HFD) (Table S1). Treatment initiated along with the beginning of HFD and contained every day to two oral doses (10 mg/kg) of resuspended Au-NPs and Au@P-NPs in drinking H_2O of animal facility throughout 8 weeks. The vehicle-treated (H_2O) groups are referred to as CD and HFD. Body weight increase and food eating were measured two times in a week. At week 8, mice were anesthetized by CO_2 asphyxiation and subsequently sacrificed prior to awakening from anesthesia. Blood was collected by cardiac puncture in heparinized (2 IU) capillary tubes, and without delay centrifuged at 3000 rpm for 30 min at 4 °C to separate plasma from cells. Plasma layer was kept at −80 °C until processing. Fat pads, namely brown, subcutaneous and visceral were cautiously abstracted together with gastrocnemius muscle, liver, lungs, kidneys, heart and pancreas (Fig. S1). The detailed methods and analyses applied to examine the gut microbial taxonomic abundances in mouse faecal samples are provided in the Supporting Information.

2.4. Total RNA extraction and qPCR analysis

We homogenized freeze-dried powdered samples of collected tissues in1 ml of QIAzol lysis reagent (Qiagen, Germany). Total RNA was extracted and purified using an RNeasy mini kit (Qiagen, Germany). cDNA was constructed with total RNA (1 μg) using the Verso cDNA synthesis kit (Thermo Fisher Scientific, India) following the manufacturer's instructions. The qPCR was carried out using SYBR Green master mix (Thermo Fisher Scientific, India) with 1:10 diluted cDNA on a 7900HT real-time system (Applied Biosystems, USA). The relative expression of genes of interest was assessed by the $\Delta\Delta_{Ct}$ method. The primers used to detect genes are structured using the program, Primer3 v.0.4.0, and gene sequences are mentioned in Table S2.

2.5. Glucose homeostasis

For insulin (INS) tolerance tests, we starved mice for 6 h (8 a.m. To 2 p.m.) at week 7. We administered ISN with a dose of 1 IU/kg through i.p. injection. We measured glycaemia (blood glucose content) by a glucometer (Roche, Germany) using the blood obtained from the tail before INS administration, and at 10, 20, 30, and 60 min after INS administration. For oral glucose tolerance test (OGTT), animals were starved overnight (8 p.m.–8 a.m.) at the end of week 6 and glucose at the dose of 1 g/kg body weight was given orally. We quantified glycaemia with a glucometer using the blood collected from the tail prior to glucose administration and at 0, 15, 30, 60, 90 and 120 min following glucose

administration. Approximately 30 μL of blood was used during OGTT for insulinaemia measurement. We measured the homeostatic model assessment of insulin resistance (HOMA-IR) index using the formula of Anhê et al. [3].

2.6. Faecal microbiota transplantation (FMT) experiments

FMT experiments were carried out with faecal resuspension (FRS) from mice fed HFD plus Au@P-NPs for 8-weeks. The harvested faecal pallets (110 mg) were transferred to anaerobic chambers for making suspension in 1x PBS (350 μL) [3]. Eight-weeks-old 14 GF mice were maintained under aseptic conditions, and animals were treated forcefully with immediately made 350 μL of FRS orally. Germ-free (GF) mice reinoculated with the faecal microbiota of HFD-fed control animals (denoted as HFD-recipients; n = 5) and Au@P-NPs-treated (denoted as Au@P-NPs recipients; n = 5). Recipient mice were first kept in metabolic cages (Sable International Systems, USA) for 4 days and then shifted to ventilated GF cages for next 10 days and maintained on less-fat (10%) containing diet during the early days of post-colonisation (PC) (Fig. S2).

The protocols applied to examine bacterial quantification by qPCR, metabolic rate, interscapular temperature, plasma bile acids, protein expression, H&E staining, primer sequences, and composition of diets are available at the online Supporting Information.

2.7. Statistical analysis

All values are presented as mean ± standard error (SE). We used one-way ANOVA with Bonferroni post hoc test (BPHT) and Kruskal-Wallis test (KWT) with Dunn's multiple comparison tests (DMCT) for parametric and non-parametric results, respectively to allocate significance to the differences among groups (SPSS 13.0, USA). We used two-way ANOVA with a BPHT (Sigmaplot, USA) when time was considered as a variable.

3. Results and discussion

We examined the morphology and size of Au-NPs and Au@P-NPs by TEM. The NPs distributed uniformly, and the average dimensions of Au-NPs and Au@P-NPs were approximately 17 nm (Fig. 1a–d). The hydrodynamic diameters of Au-NPs and Au@P-NPs were 27.6 and 29.1 nm, respectively and the corresponding zeta-potential values were −12.4 mV for Au-NPs and −15.6 mV for Au@P-NPs (Table S3). The polydispersity index (PDI) of Au-NPs was 0.278, while Au@P-NPs revealed PDI of 0.286, indicating the monodispersity of Au@P-NPs. To determine the stability of synthesized NPs, PDI values were measured after twelve months of storage at 25 ± 1 °C. Au@P-NPs revealed excellent monodispersity (PDI-0.293), while PDI of Au-NPs increased from 0.278 to 1.138 (Table S2), demonstrating the capability of phytochemicals-rich *C. verum* bark extract to act as superior capping and stabilizing agents than citrate. An absorption peak of Au@P-NPs was about 531 nm in the UV spectra (Fig. S3), which might be due to the SPR of gold-based NPs [42]. The appeared peaks at 3593, 3174, 1607, 1441 and 1047 cm^{-1} were denoted to O–H bond stretching vibration [43], C–H and alkene stretches [44], C–O stretch, the in-plane bending of the O–H group [44] and C–O bond stretching vibration [44], respectively in the FTIR spectrum of Au@P-NPs (Fig. 1e). The –C═O stretching and –OH stretching bands corresponded to the polyphenolic compounds [45] while the C–H stretching indicated the presence of aromatic compound(s) of *C. verum* [46], indicating that the phytochemicals of *C. verum* were capped on Au@P-NPs. It has been reported that the interaction of NPs-phytochemicals could occur through the electrostatic repulsion force of negatively charged polyphenolic compounds [47].

After corroboration of involvement of phytochemicals of *C. verum* in capping of Au@P-NPs, 1D ^{1}H (proton) NMR analysis was performed to study the details of anti-obesity compounds present on the surface of Au@P-NPs. We identified 13 metabolites, viz., 3-hydroxybutyrate, cinnamyl acetate, glucose, myoinositol, glycerol, galactose, ferulic acid, catechin, rutin, pyrogallol, *p*-coumaric acid, cinnamic acid and cinnamaldehyde which were involved in the coating of NPs (Fig. 2; Table 1). Although galactose is the major component of Au@P-NPs, several studies have reported that galactose and its derivatives act as linker agents to assemble various functional agents on the surface of metal NPs [48,49]. As such, the content of galactose present on the surface of Au@P-NPs was so less that it was unlikely to cause hyperglycemic-mediated obesity [50] rather it might have favoured gut microbes responsible for maintaining gut-microbiota-bile acid axis. In addition, *p*-coumaric acid [38], pyrogallol [51], cinnamaldehyde [52], ferulic acid [53] and cinnamic acid [54,55] present on the surface of Au@P-NPs have been reported for inducing thermogenesis and brown adipose tissue (BAT) activation in adipose tissues (ATs) to provide anti-obesity effects. Similarly, other cinnamyl acetate, rutin and catechin are known for anti-inflammatory activity [16,56,57] which can regulate metabolic inflammation in ATs of HFD-fed mice.

We administered Au-NPs and Au@P-NPs orally once a day to the obese mice induced by HFD throughout 8-weeks at a concentration of 10 mg/kg to assess their beneficial effect on obesity and related metabolic disorders. Au@P-NPs treatment prevented gain in HFD-induced body weight from day 14 onwards (Fig. 3a and b) and these results were not related to alterations in energy intake (Fig. 3c). The accumulation of fat in ATs is often related to obesity and related disorders [3,36]. Therefore, we examined whether the Au@P-NPs-induced prevention of weight gain is associated with alterations in ATs. Au@P-NPs prevented fat accumulation in all ATs namely, epididymal white AT (eWAT), retroperitoneal white AT (rWAT), mesenteric white AT (mWAT), inguinal white AT (iWAT) and interscapular brown AT (iBAT) (Fig. 3d). Treatment of Au@P-NPs did not affect the weight of heart, gastrocnemius and pancreas as well as length of intestine, and caecum quantity (Fig. S4a–f). When compared with the CD group, liver weight in HFD-fed group significantly raised, but HFD-persuaded liver weight and hyperlipidemia were markedly prevented by Au@P-NPs administration (Fig. 3e), as revealed by reduced contents of triglyceride, total cholesterol and LDL-c in both liver homogenate (Fig. 3f) and plasma (Fig. 3g) of Au@P-NPs group against HFD control group, measured by colorimetric kits. We noticed non-significant difference in everyday faecal energy production between Au@P-NPs-treated and HFD control groups, indicating that Au@P-NPs did not modify food assimilation (Fig. 3h). Au@P-NPs treatment enhanced energy consumption, which was not related to reinforce physical movement (Fig. 3i; Fig. S4g–l), ensuring a smaller amount of energy available for deposition (Fig. 3j). In line with elevated oxygen utilization, Au@P-NPs-treated animals revealed an increasing interscapular temperature (36.66 °C ± 0.07) than HFD-fed (35.69 °C ± 0.08) animals (Fig. 3k). On the other hand, Au-NPs did not impede HFD-induced weight gain and fatty liver parameters. Au@P-NPs were much more efficient in the prevention of weight gain, adiposity and dyslipidemia by accelerating energy consumption and thermogenesis than Au-NPs. These findings indicate that the involvement of anti-obesity phytochemicals of *C. verum* in coating of the NPs which play a key role in preventing the weight gain and inducing thermogenesis by Au@P-NPs in HFD-induced obese mice.

We next studied the levels of interleukin-1 beta (IL-1β), IL-6 and interferon-γ (INF-γ) in serum using ELISA kits to assess metabolic inflammation in the AT of HFD-fed mice without and with treatments. The mice belonging to HFD control and Au-NPs-treated groups exhibited greater IL-1β, IL-6 and INF-γ levels than the Au@P-NPs group (Fig. 4a–c). We observed reduced levels of C–C chemokine ligand/RANTES, a chemokine, VEGF (vascular endothelial growth factor), and chemokine ligand 2 (CCL2/MCP-1) in the Au@P-NPs group compared to the HFD control group (Fig. 4d–f). Corresponding to decreased CCL2, an essential regulator of macrophage infiltration in the AT, we observed reduced expression of *Adgre* (F4/80) mRNA (Fig. 4g). Au@P-NPs revealed decreased adipocyte size (Fig. S5a–c) and it has been reported that large adipose cells trigger an inflammatory cascade in ATs [58]. Au@P-NPs

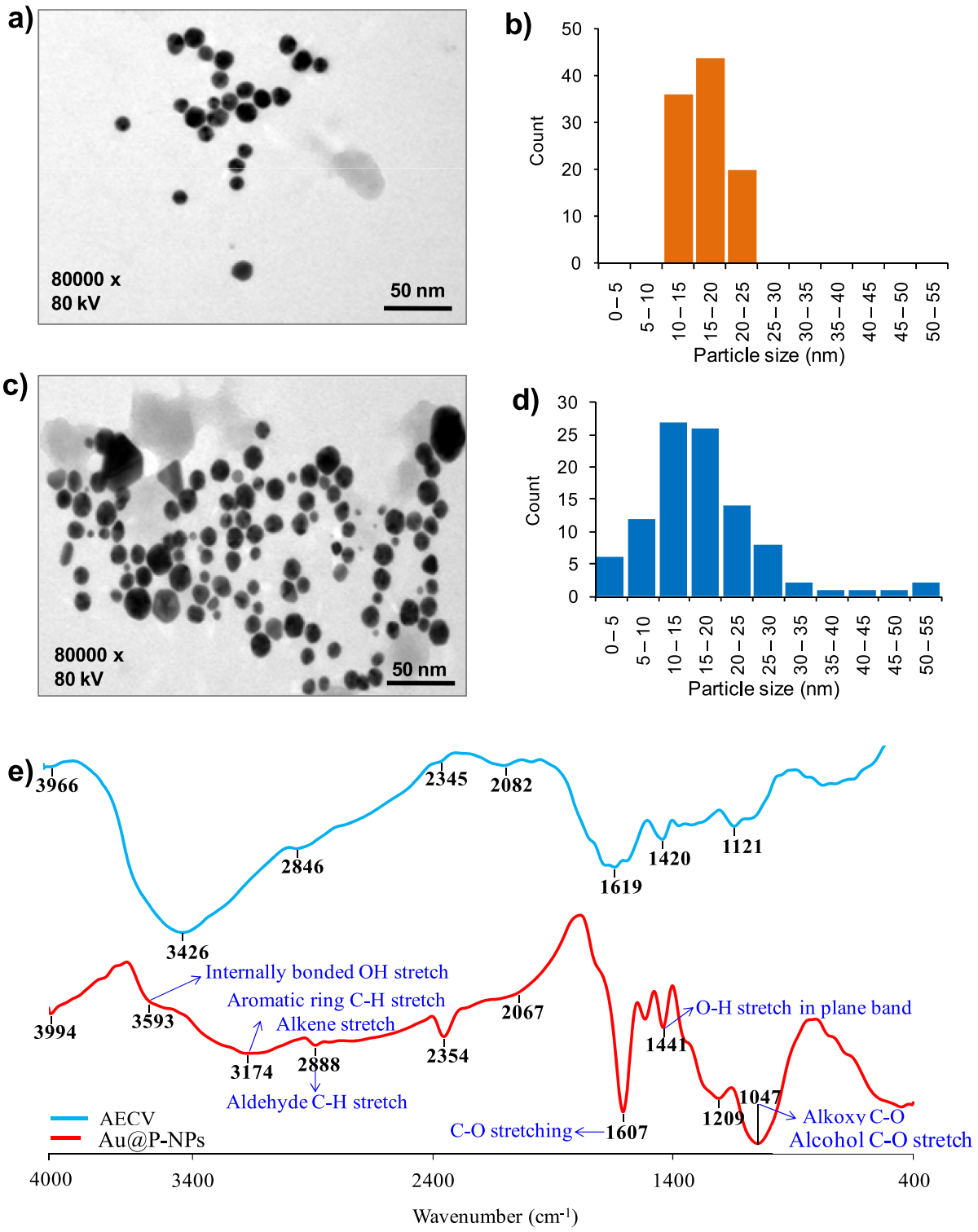

Fig. 1. Morphology of NPs. (a) TEM image of Au-NPs. (b) Size distribution of Au-NPs. (c) TEM image of Au@P-NPs. (d) Size distribution of Au@P-NPs. (e) FT-IR spectra of AECV and Au@P-NPs.

administration also obviated metabolic endotoxaemia, as showed by reduced LPS concentration in mice bloodstream (Fig. 4h), suggesting regulatory effect of Au@P-NPs on AT and circulatory cytokines.

While fasting blood glucose did not change significantly between Au-NPs and HFD control groups (Fig. 4i), Au@P-NPs treatment did obviate fasting hyperinsulinemia (Fig. 4j), resulting in the enhanced fasting insulin sensitivity (IS) as revealed by reduced HOMA-IR, a technique applied to measure β-cell function and insulin resistance (Fig. 4k). OGTT revealed that Au@P-NPs improved glucose tolerance (Fig. 4l and m) and restricted HFD-induced hyperinsulinemia (Fig. 4n and o). The IS 10 min after subcutaneous injection of insulin got improved in Au@P-NPs group as compared to HFD control group (Fig. 4p). In summary, these results suggest that Au@P-NPs treatment improves glucose homeostasis and IS by preventing the HFD-induced obesity and visceral fat deposition and inflammation.

Since obesity is the results of high fat/or sucrose induced imbalance

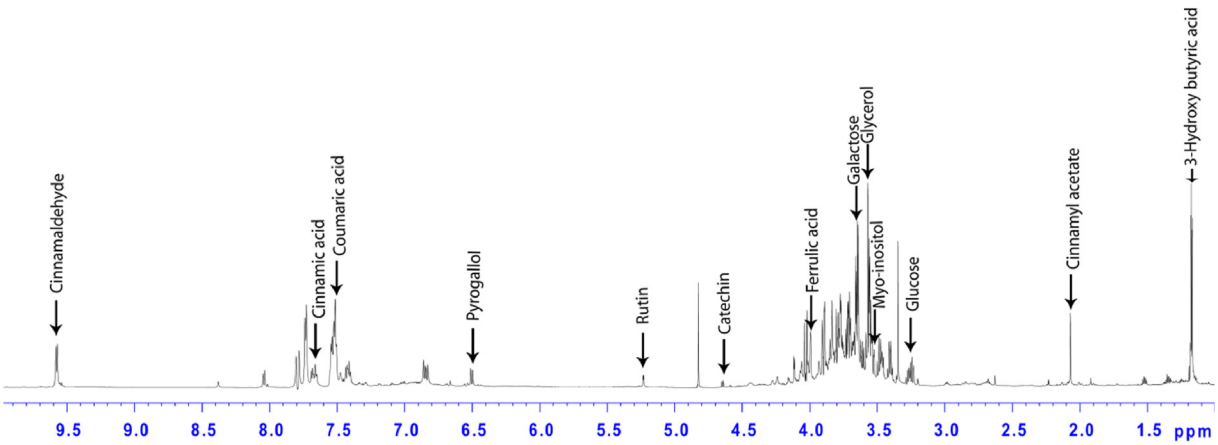

Fig. 2. Quantification of bioactive compounds of *C. verum* involved in capping of Au@P-NPs using NMR analysis. The Au@P-NPs was centrifuged at 10,000 rpm for 20 min at 4 °C. The obtained NPs were washed thrice using Milli-Q water, fractionated using ethyl acetate, and recorded 1D ^{1}H proton NMR spectra.

in gut microbial community, remodeling of gut microbial diversity is an important strategy in the prevention of obesity [3,59]. Mounting evidences have associated with the reduction of beneficial gut microbiota in obese people [8,10,11]. To confirm the consistency of the microbial profile, faecal specimens were collected at the end of the study and at the beginning of the study after acclimatization of mice on a CD. We sequenced 16 S rRNA genes by Illumina MiSeq platform, and assessed the gut microbial profile as sequenced, V3–V4 region of 16S rRNA genes using a 2 × 300PE v3 sequencing kit. Principal coordinate analysis (PCoA) showed that though all specimens of CD-fed group clustered at baseline, 8 weeks of HFD feeding severely altered intestinal microbial profile (Fig. 5a). Au@P-NPs-administered group, however, clustered partly at a distance of HFD control group specimens, signifying fundamental alterations in Au@P-NPs intestinal microbial profile (Fig. 5a). Au@P-NPs administration obviated the HFD-induced reduction in gut microbial richness, as indicated by Chao1 index (Fig. 4b) and F/B ratio (Fig. 5c and d), two key indicators of gut microbial diversity [9,60]. At genus level, Au@P-NPs protected the HFD-induced reduction in *Akkermansia*, *Bifidobacterium*, *Barnesiella* and *Proteobacteria*, and decreased the relative abundance of *Lactobacillus*, *Streptococcus*, *Acinetobacter* and *Papillibacter* (Fig. 5e). We observed the most of the decline in Firmicutes in the gut microbiota of Au@P-NPs-treated group as compared to HFD control group (Fig. 5d).

The linear discriminant analysis effect size (LEfSe, an algorithm used for biomarker discovery and plotting in microbiome studies) method ranked *Bacteroides*, *Parabacteroides* and *Barnesiella* coupled with a foremost reduction in operational taxonomic units (OTUs, applied to categorize groups of closely related individuals) designated to *Lactobacillus* spp. and *Streptococcus* spp. as the major attributes distinguishing faecal microbial populations of Au@P-NPs group from that of HFD control group (Fig. 5h). As we noticed a propensity towards increase of *Akkermansia muciniphila* and *Bifidobacterium* in Au@P-NPs group (Fig. 5e), we quantified these bacteria by qPCR technique and detected a foremost enhance in their population in Au@P-NPs group (Fig. 5i and j). Increasing abundances of *A. muciniphila* and *Bifidobacterium* were reported demonstrating the metabolic benefits of these gut bacteria [61,62]. Several researchers have earlier confirmed the relationship between consumption of dietary polyphenol-rich extracts and enhanced abundance of *Bifidobacterium* and *A. muciniphila* [63]. Our study also revealed the presence of polyphenolic compounds of *C. verum* on the surface of Au@P-NPs, which have known positive effects on *A. muciniphila*. Polyphenolic compounds found in the cell wall of certain plants increase the abundance of *A. muciniphila* and other probiotic bacteria [3,64,65]. Au@P-NPs is also coated with various polyphenolic compounds, such as cinnamic acid, cinnamaldehyde, ferulic acid, rutin, and catechin seem to promote the growth of beneficial gut bacteria, particularly *A. muciniphila* and *Bifidobacterium* in vivo. In early weaned rats, cinnamic acid and cinnamaldehyde from *C. verum* have been reported to decrease cardiometabolic risk through glucose uptake inhibition and appetite modulation by remodeling gut microbiome [66,67]. Similarly, rutin, another polyphenolic compound was reported to attenuate gut dysbiosis and inflammation in paneth cells of obese mice [68]. The positive effect of catechin, another dietary flavonoid present in green tea and *C. verum*, on gut microbes is also well-established in several pre-clinical studies [69,70]. Thus, the presence of above ingredients of *C. verum* on the surface of NPs with proven gut microbial regulatory effects provides an explanation how Au@P-NPs modulates gut microbiota of HFD-fed mice.

Table 1
Identification and quantification of bioactive compounds on the surface of Au@P-NPs

Chemical shift (ppm)	Multiplicity	Metabolite	Content (μg/mg Au@P-NPs
1.19	d	3-Hydroxybutyrate	1.81 ± 0.11
2.07	s	Cinnamyl acetate	0.66 ± 0.35
3.26	t	Glucose	2.44 ± 0.15
3.53	dd	Myoinositol	4.48 ± 0.27
3.59	m	Glycerol	3.75 ± 0.24
3.68	dd	Galactose	14.73 ± 1.16
3.97	s	Ferulic acid	1.14 ± 0.11
4.46	d	Catechin	0.43 ± 0.02
5.22	d	Rutin	2.11 ± 0.16
6.5	d	Pyrogallol	0.96 ± 0.04
7.5	m	*p*-Coumaric acid	6.04 ± 0.31
7.69	m	Cinnamic acid	1.46 ± 0.13
9.58	d	Cinnamaldehyde	2.68 ± 0.16

Results are presented as the mean ± SE.
d, doublet; **s**, singlet; **t**, triplet; **dd**, doublet of doublets; **m**, multiplet.

While OTUs designated to the genera Bacteroides and Parabacteroides (Fig. 5h), their abundances were considerably low (Fig. 5e). We thus decided to focus on the significant Au@P-NPs-associated actions, particularly on the phytotypes such as *Lactobacillus*, *Streptococcus*, *Acinetobacter*, *A. muciniphila, Barnesiella* and *Bifidobacterium.* Besides, no noticeable histological injury in major organs such as liver, lungs, kidney, heart and pancreas (Fig. 6) and no significant alteration in the level of blood serum parameters (Table 2) were observed in 8-weeks-old mice treated with Au@P-NPs as compared to CD-fed group, demonstrating the biocompatibility of the Au@P-NPs.

As bile acids are known to regulate glucose, lipid and energy metabolism in BAT and skeletal muscle [18,71], we wanted to assess whether alterations in the bile acids profile can be related to the impacts observed in Au@P-NPs-treated group. Although the relative proportion of

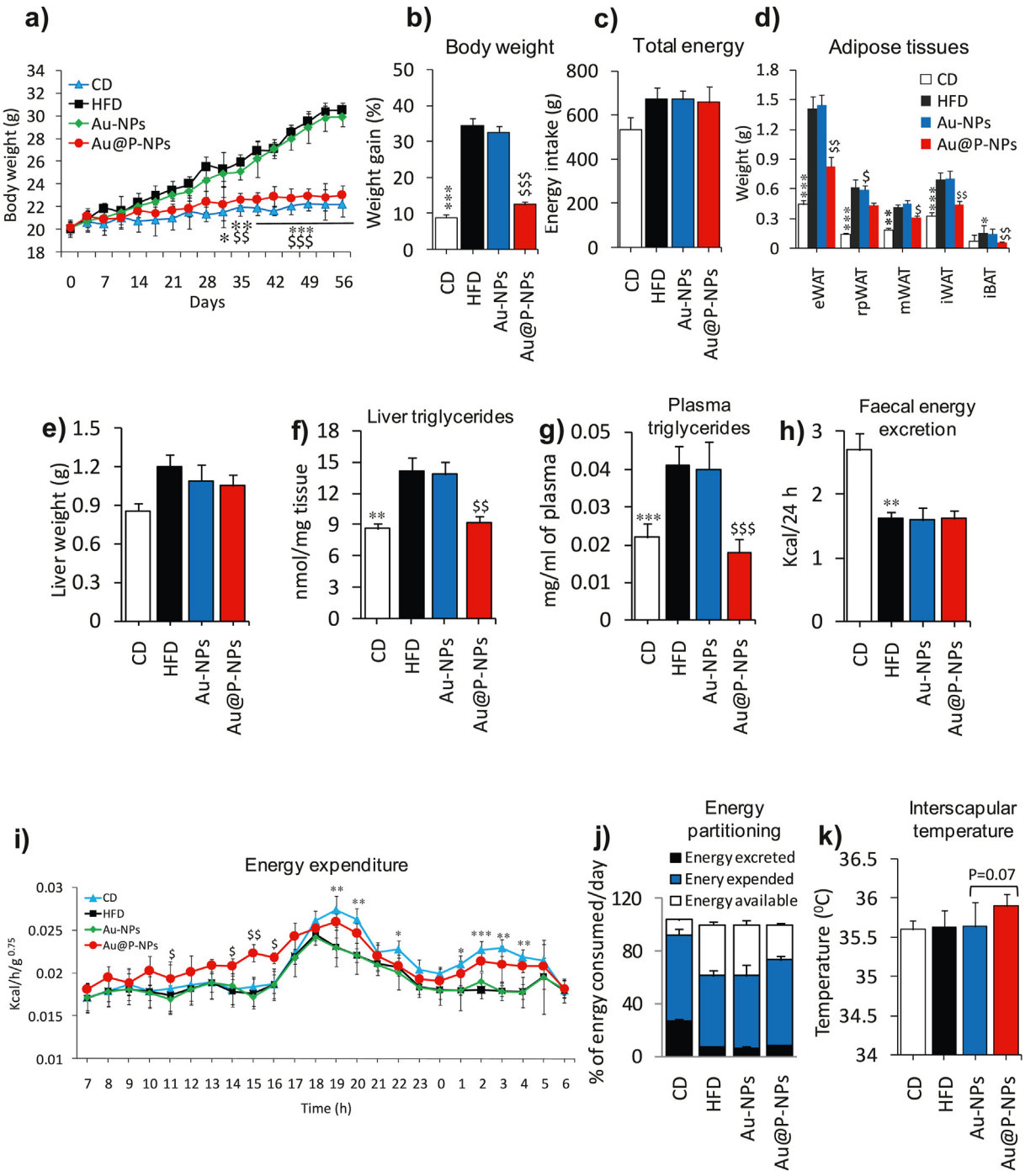

Fig. 3. Treatment of Au@P-NPs and Au-NPs on a mice obesity model induced by HFD. We fed the mice either a CD or HFD and treated with daily dose of Au@P-NPs and Au-NPs at the concentration of 10 mg/kg body weight for 8 weeks. (a) Body weight in grams. (b) Body weight in percentage. (c) Energy consumption. (d) Weight of eWAT, rWAT, mWAT and iWAT together with iBAT, which indicated the level of fat storage, in adipose tissues. (e) Liver weight. (f) Content of liver triglycerides. (g) Content of triglycerides in the blood after 6 h of starvation, an indicator of hyperlipidemia. At week 5, animals were placed in metabolic cages and assessed (h) faecal energy excretion and (i) energy expenditure. The connection between metabolic rate and body mass was normalized using the metabolic body size (ie, body mass$^{0.75}$) and measured (j) energy partitioning and (k) interscapular temperature. (a, i) Two-way frequent measurements ANOVA with BPHT. (b–h, k) One-way frequent measurements ANOVA with BPHT. $^{*}P < 0.05$, $^{**}P < 0.01$ and $^{***}P < 0.001$ for CD against HFD; $^{\$}P < 0.05$, $^{\$\$}P < 0.01$ and $^{\$\$\$}P < 0.001$ for Au@P-NPs against HFD.

ω-muricholic acid (ω-MCA; a secondary bile acid) was higher in the plasma of Au@P-NPs-treated group than the HFD-fed group, the abundance of conjugated bile acids such as tauro-α-murocholic acid (TαMCA) and tauro-β-murocholic acid (TβMCA) were lesser in the former group (Fig. 7a and b). Besides, the relative proportions of unconjugated bile acids, viz., CDCA (chenodeoxycholic acid), DCA (deoxycholic acid), hyodeoxycholic acid and UDCA (ursodeoxycholic acid) were greater in the plasma of Au@P-NPs-treated group than the HFD-fed control group (Fig. 7b; Fig. S6a-h). Bile acid content in faecal material was similar in HFD-fed control and Au@P-NPs-treated groups (Fig. 7b; Fig. S6a-h), indicating that changed circulatory bile acids in Au@P-NPs group was related to variation in bile acid production rather than excretion/re-uptake. Based on the obtained results, we cerebrated that farnesoid X receptor (FXR)-stimulating bile acid synthesis may

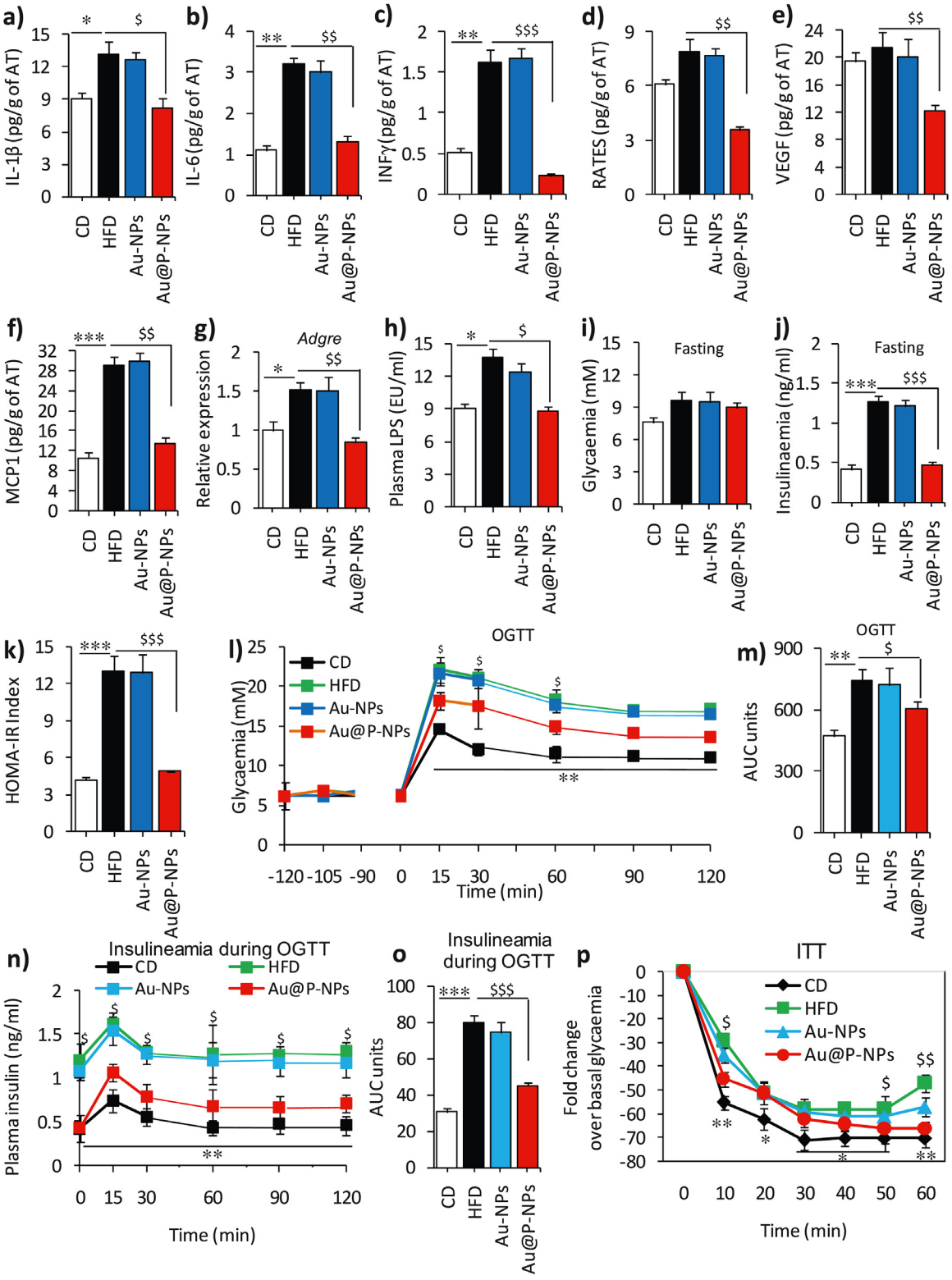

Fig. 4. Treatment of Au@P-NPs and Au-NPs on inflammation and glucose homeostasis in HFD-fed mice. Protein lysates of eWAT of mice were used to measure (a) IL-1β, (b) IL-6, (c) INF-γ, (d) RANTES, (e) VEGF and (f) MCP-1. (g) Relative mRNA expression of *Adgre* in eWAT by qPCR. (h) LPS content in blood plasma of 6 h starved animals. Animals were starved from 6 p.m. to 6 a.m. (12 h) at week 6 and subjected to OGTT. NPs were orally given 120 min before to the experiment, and the status of glycaemia was measured 15 min after NPs treatment to examine potential alterations in glycaemia related with sugars present in Au@P-NPs to observe likely alterations in glycaemia linked with sugars of *C. verum* present in AECV. (i) Glycaemia (fasting) index. (j) Insulinaemia (fasting) index. (k) HOMA-IR. (l) OGTT/glycaemia (nM). (m) OGTT in terms of an area under the curve (AUC). Blood samples were collected during OGTT and employed after glucose administration to measure (n) Insulinaemia during OGTT and (o) Insulinaemia in terms of AUC. Animals were starved for 6 h at week 7 and (p) ITT (insulin tolerance test) was performed after insulin injection at the dose of 1.0 IU/kg through i.p. route. (l, n and p) Two-way frequent measurements ANOVA with BPHT. (a–k, m and o) One-way frequent measurements ANOVA with BPHT. $^{*}P < 0.05$, $^{**}P < 0.01$ and $^{***}P < 0.001$ for CD against HFD; $^{\$}P < 0.05$, $^{\$\$}P < 0.01$ and $^{\$\$\$}P < 0.001$ for Au@P-NPs against HFD.

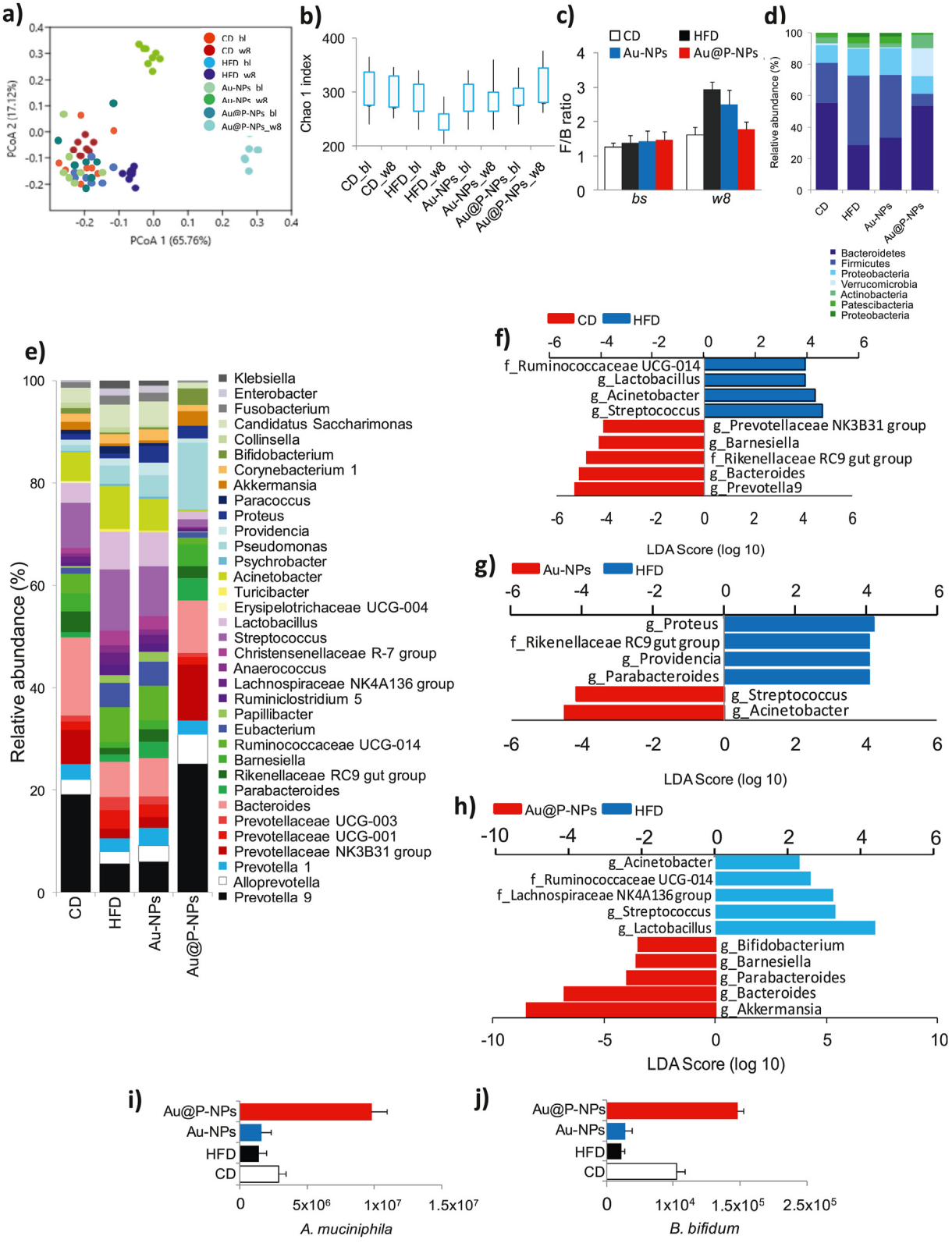

Fig. 5. Effect of Au@P-NPs on obesity-associated gut microbiota imbalance in HFD-fed mice. At week 8, faecal pellets of indicated treatments were collected. Faecal samples were also harvested during the last week of adaptation on a CD (indicated to bl), before the administration of the HFD or Au@P-NPs. After getting good quality of genomic DNA, 16 S rRNA gene-based gut microbiota profiling was carried out. (a) PCoA. (b) Chao1 index at OTU level. (c) F/B ratio. The relative richness of phylotypes at (d) phylum and (e) lowest taxonomic level (LTL) attained. LEfSe was figured out to investigate the taxa within the LTL likely that more sturdily distinguish between the gut microbiota of (f) CD *vs* HFD, (g) Au-NPs *vs* HFD, and (h) Au@P-NPs *vs* HFD. (i) qPCR amplification of *A. muciniphila* normalized by 3×10^9 copies of 16 S (total bacteria) in faecal sample. (b–e) KWT with DMCT. (i) One-way frequent measurements ANOVA with a BPHT. $^{*}P < 0.05$, $^{**}P < 0.01$ and $^{***}P < 0.001$ for CD *vs* HFD; $^{\$}P < 0.05$, $^{\$\$}P < 0.01$ and $^{\$\$\$}P < 0.001$ for Au@P-NPs *vs* HFD.

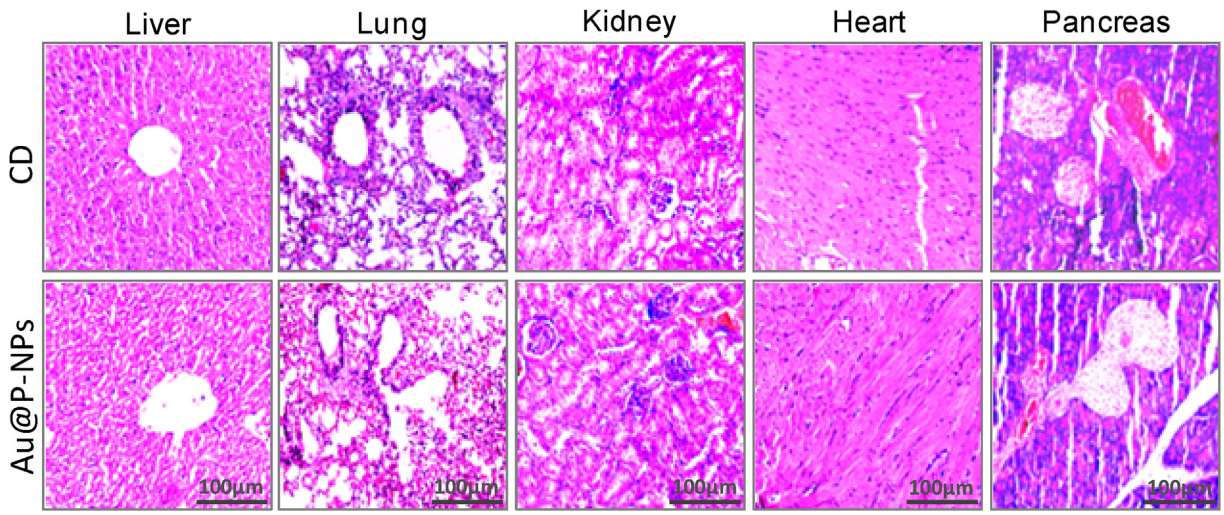

Fig. 6. Biocompatibility of Au@P-NPs with animals after 8 weeks of oral administration. H&E staining of mice tissues, namely liver, lung, kidney, heart, and pancreas.

recompense for the prohibitory action of decreased bile acid pool size, thus hampering the FXR-led negative reaction link regulatory bile acid profile in Au@P-NPs-treated group and retaining the contents of plasma bile acids lower in comparison to HFD-fed control group. While more studies in the future are required to fully decode the mode of actions by which Au@P-NPs affect bile acid equilibrium, it is of primary concern that Au@P-NPs administration decreased circulatory bile acid synthesis in HFD-fed animals. Changed bile acid profile may regulate to reform the gut microbiota in Au@P-NPs-treated animals. Bile acids act as antimicrobial agents and the bile acid pool noticed on HFD feeding, which increases the abundance of taurine-conjugated bile acids (eg, TαMCA and TβMCA) in the enterohepatic circulation [3]. The presence of bile acids is linked with proliferation of bile-acid-resistant *Lactobacillus* species in the intestine atmosphere [72]. The decreased bile acid pool size observed in Au@P-NPs-treated group might have reduced the *Lactobacillus* population size in the gut environment.

Bile acids are microbial-secreted metabolic regulators that bind to FXR to activate *Nr0b2* (Shp1) blocking the synthesis of bile acids in the liver and uptake in the ileum [73]. Activated FXR is also responsible for enhanced secretion of *Fgf15* (fibroblast growth factor 15) in ileum, that reduces bile acid formation in the liver via binding with *Fgfr4* [74]. Therefore, we hypothesized that Au@P-NPs treatment may down-regulate *Nr0b2* expression. Next, we found that the Au@P-NPs were capable to decrease *Nr0b2* mRNA expression in the ileum of animals. This Au@P-NPs impact was also adequate to reduce the mRNA expression of *Fgf15* and FXR-regulated genes, viz., *Slc51a* and *Slc51b* in the ileum of treated animals (Fig. 7c). Moreover, Au@P-NPs treatment reduced *Cyp7a1* mRNA expression in the liver versus HFD-fed control group (Fig. 7d), suggesting the decreased bile acid profile observed in Au@P-NPs-administered group which might be responsible for reducing FXR expression in the mice ileum. This conclusion is supported by decreased mRNA expressions of *Nr0b2* and *Fgf15* in ileum of Au@P-NPs group [75,76]. As we noticed a key reduction in the content of FXR antagonists (eg, TαMCA, TβMCA) along with an enhanced FXR agonist (eg, CDCA) in the bile acid profile of Au@P-NPs-treated group, we assumed that such FXR-activatory bile acid pool may repay for the impending result of decreased bile acid profile size, thus disturbing the FXR-mediated negative reaction directing bile acid synthesis in Au@P-NPs group and maintaining the contents of circulating bile acids lower than the HFD-fed control group. While detailed investigations are needed to completely unravel the mode of actions by which Au@P-NPs affect bile acid homeostasis, it is noteworthy that Au@P-NPs treatment decreased plasma bile acid pool in the HFD-fed animals.

We detected a notable increase in the mRNA expressions of *Ucp1* (uncoupling protein 1) and *Dio2* (deiodinase 2) in both iWAT and BAT of Au@P-NPs-treated group (Fig. 7f and g). Further supporting iWAT browning, Au@P-NPs group revealed a trend of upregulated mRNA expression of *Pparg2* (peroxisome proliferator-activated receptor γ-2), *Prdm16* (PR domain containing 16) and *Ucp1* in iWAT compared to the HFD-fed control group (Fig. 7f). With enhanced BAT activity, Au@P-NPs increased the mRNA expression of *Pparg2* and *Pgc1a* (PPARγ coactivator 1α) in the BAT as compared to HFD-fed control mice (Fig. 7g). The *Fgf15*, an intestinal hormone has been reported to activate the process of thermogenesis and browning of WAT by inducing *Fgfr4* activation [77]. Constantly, we noticed higher *Fgfr4* mRNA expression in the iWAT than in the eWAT and BAT of Au@P-NPs-treated group (Fig. 7e-g), suggesting that increased browning of subcutaneous white fat in this group is linked to enhanced sensitivity to *Fgf15*. We observed a strong correlation between the mRNA expression profiles of many genes implicated in activation of BAT and iWAT browning (Fig. 7h). *Ucp1* and *Dio2* genes in BAT had strong correlation with *Ucp1* and *Dio2* in iWAT. In addition, within the BAT, *TGR5* was strongly correlated with *Pgc1a,* and within the iWAT, *Ucp1* and *Dio2* were correlated with *Dio2* and *fgfr4*, respectively. Watanabe et al. in their study concluded that *A. muciniphila* is positively correlated with plasma CDCA and particularly the secondary bile acids, viz., DCA and UDCA that worked via *TGR5* to increase the brown lipocytes and non-shivering thermogenesis (heat generation owing to metabolic energy alteration by burning of WAT) by promoting intracellular thyroid hormone activation [18]. Thus, the circulatory bile acids levels observed in our study in Au@P-NPs-treated animals were related to the increased BAT activation and browning of subcutaneous WAT through enhanced energy expenditure which might have been modulated through the gut microbiota.

However, quantifying how dietary polyphenolic compounds alter the intestinal microbial atmosphere to support the growth of *A. muciniphila* needs additional study. The interaction between this bacterium and bile acid pool size also needs to be investigated. No pathway connection to deconjugation/dehydroxylation of bile acid in the genome database (KEGG) of *A. muciniphila* was found. The capability of *A. muciniphila* to transform and resist to the antimicrobial action of various bile acids though indicated, further lab-based validations are needed. Although the direct involvement of changed bile acid profile size and composition observed in Au@P-NPs-treated group in increasing energy expenditure needs further study, the present study did bring novel insights into the cross-talk between bile acid and gut microbiota, and its association with the anti-obesity effects of phytochemicals-functionalized AuNPs.

We also assessed whether alterations in lipolytic/lipogenic event also contribute to decreased fat accumulation observed in Au@P-NPs-treated

Table 2
Profiling of blood serum parameters in mice after 8 weeks treatment of CD and Au@P-NPs

Parameter	CD	Au@P-NPs
Blood biomarkers:		
RBCs (10^{12}/L)	4.83 ± 0.29	5.14 ± 0.028
WBCs (10^{9}/L)	7.37 ± 0.55	7.88 ± 0.62
HGB (g/dL)	14.4 ± 1.13	14.1 ± 1.04
CRP (mg/L)	0.97 ± 0.052	1.03 ± 0.021
BG (mg/dL)	101.2 ± 8.44	104.1 ± 8.28
Liver biomarkers:		
ALT (U/L)	82.2 ± 7.24	87.1 ± 8.52
AST (U/L)	124.4 ± 11.5	131.4 ± 14.1
ALP (U/L)	29.7 ± 1.93	28.7 ± 1.37
TB (mg/dL)	0.69 ± 0.041	0.72 ± 0.041
Kidney biomarkers:		
Creatinine (mg/dL)	1.54 ± 0.14	1.51 ± 0.013
BU (mg/dL)	17.9 ± 1.38	18.9 ± 1.72
Lipid biomarkers:		
TC (mg/dL)	81.9 ± 8.16	85.1 ± 7.61
HDL-c (mg/dL)	42.4 ± 4.16	43.7 ± 5.1
TG (mg/dL)	93.6 ± 7.51	92.8 ± 9.72

Results are presented as the mean ± SE.
RBCs, red blood cells; WBCs, white blood cells; HGB, haemoglobin; CRP, C-reactive protein; ALT, alanine aminotransferase; AST, aspartate aminotransferase; ALP, alkaline phosphatase; TB, total bilirubin; BU, blood urea; TC, total cholesterol; HDL-c, high density lipoprotein cholesterol; TG, triglyceride; BG, blood glucose.

group. Besides increased plasma-free glycerol (Fig. 7i) and upregulated expression of *Ppara* gene in both eWAT and iWAT of Au@P-NPs group (Fig. 7e and f), we observed higher expression of *Pnpla2*, an adipose triglyceride lipase in eWAT and iWAT (Fig. 7e and f). Also, we noticed the downregulation of lipoprotein lipase (LPL) inhibitor fasting-induced adipose factor (*Fiaf*) and monoacylglycerol lipase (*Mgl1*) in ileum of Au@P-NPs group (Fig. 7c). These results highlight the enhanced fat breakdown/oxidation process fuelled by greater triglyceride removal. We observed downregulated protein expression of CD36 (cluster of differentiation 36) and FAS (fatty acid synthase) in the eWAT (Fig. S7a), and reduced FABP4 (fatty acid-binding protein 4) and FAS in the iWAT of Au@P-NPs-administered group (Fig. S7b). Au@P-NPs treatment failed to affect the protein expressions of CD36, PPARγ (peroxisome proliferator-activated receptor-γ) and acetyl-CoA carboxylase (ACC) in the iWAT (Fig. S7d). Similarly, no difference was also observed between Au@P-NPs and HFD-fed control groups for the protein expressions of PPARγ, FABP4 and ACC in the eWAT (Fig. S7c). The results showed that, besides elevated energy expenditure, Au@P-NPs-treated group had enhanced fat breakdown process and reduced lipid formation in both visceral and subcutaneous fat depositories, which resulted in low weight gain in HFD-induced obese mice [3,36].

Firmicutes and Bacteroidetes are the key phyla that constitute more than 90% of gut microbiota in mice. Their relative population is directly associated with the obesity and metabolic disorders of the host [9,78,79]. We carried out FMT experiments on GF mice, colonized either with the faecal microbiota of Au@P-NPs or HFD donor mice. Recipient animals were fed a low-fat diet to eliminate a key obesogenic effect and hence to allow for an experimental effect of FMT on body weight in the short-term. During days 1, 2 and 3 PC of gut microbiota, Au@P-NPs receiver mice lost 3.7%, 4.9% and 2.1% of their initial body weight (IBW), respectively (Fig. 8a). On the other hand, HFD receiver animals revealed 2.9% body weight gain on day 1 PC followed by a 3.4% and a 2.3% gain of their IBW on days 2 and 3, respectively (Fig. 8a). This stemmed in noteworthy variations in body weight increase between Au@P-NPs and HFD receivers on days 1 and 2 PC and a trend to be sustained at day 3 PC. We observed no variation in energy intake of faecal energy expenditure between Au@P-NPs and HFD receiver groups (Fig. 8b). We performed indirect calorimetry analyses during the initial days PC which showed a significant enhancement in energy expenditure not linked to physical movement on days 1 and 2 PC. This impact was decreased on day 3 PC and totally vanished on day 4 PC (Fig. 8c; Fig. S8a-f). Illumina MiSeq analysis of 16S rRNA genes showed dissimilar gut bacterial populations in Au@P-NPs-receiver and HFD-receiver on day 2 PC (Fig. S8h). Bacterial populations grouped further separately on day 3 PC, that was revealed greater resemblance between HFD-receiver and Au@P-NPs-receiver intestinal microbiota on day 3 PC (Fig. S8i). The variations observed on day 2 PC were mainly led by a greater population of Verrucomicrobia (Fig. 8d) and lower F/B ratio (Fig. 8g). The enhanced population of Verrucomicrobia in Au@P-NPs receivers was intensified on day 2 PC, touching significant levels, and decreasing significantly on day 3 PC (Fig. 8d). As Verrucomicrobia phylum is exclusively represented by *A. muciniphila* in the gut microbiota of rodents and humans [80], the closing was as plentiful as the previous in Au@P-NPs receivers in contrast to HFD receivers for the period of gut colonisation (Fig. 8e). Moreover, 16S rRNA gene-based profiling at lesser taxonomic level on day 1 PC showed lower abundance of *Streptococcus*, *Acetinobacter* and *Corynobacterium*-1 in Au@P-NPs receivers in comparison to HFD-receivers (Fig. 8e and f). Existence of *Barnesiella* got elevated in Au@P-NPs receivers on days 1 and 2 PC (Fig. 8e and f). On day 2, Au@P-NPs recipients exhibited higher abundances of *A. muciniphila* and *Bifidobacterium* and lower proportions of *Lactobacillus* and *Acinetobacter* (Fig. 8e and f). On day 3 PC, enhanced supremacy of *Blautia*, *Prevotellaceae* UCG-001, *Rikenellaceae RC9* and *Ruminiclostridium* 5 in Au@P-NPs receivers significantly decreased the differences between the intestinal bacterial populations of animals reestablished with faecal resuspensions of Au@P-NPs-administered and HFD-fed donor animals (Fig. 8e and f). The gut microbiota of HFD and Au@P-NPs receivers was usually dissimilar with that of donor groups (Fig. 4d–g). The exemptions were the elevated proportion of *Bifidobacterium* and *Barnesiella* on days 1 and 2 PC, lower *Streptococcus* on day 1 PC and higher *A. muciniphila* on day 2 PC, characters noticed in Au@P-NPs receivers and also seen in Au@P-NPs-administered donor groups. The results recommend that though short-term colonisation is not sufficient to set up a steady gut microbiota similar to donor groups, a small number of taxa abundant in Au@P-NPs-administered group faecal microbial communities were adequate to enhance energy expenditure in the used mouse model. FMT experimentations also showed that the gut microbiota of Au@P-NPs-administered animals could moderately colonize in GF recipient animals.

We performed qPCR to examine the proportion of foremost phylotypes increased by Au@P-NPs-treated group in faecal samples of HFD receivers. The lower abundance of *Streptococcus* spp and enhanced proportion of *A. muciniphila* and *Bifidobacterium* were noticed in the faecal samples of Au@P-NPs receivers as compared to HFD receivers on day 1 PC (Fig. 8h–j). Interestingly, both *A. muciniphila* and *Bifidobacterium* stayed considerably abundant in the fæces of Au@P-NPs receivers as compared to HFD receivers on days 2 and 3 PC (Fig. 8i and j). The abundance of *Barnesiella* was found higher on day 2 PC in Au@P-NPs receivers (Fig. 8k). The abundance of *Lactobacillus* was noticed lower on day 2 PC in Au@P-NPs receiver mice (Fig. 8l). Similarly the abundance of *Acinetobacter* and *Parabacteroides* was found lower on day 2 PC in Au@P-NPs receivers in comparison to HFD-receivers (Fig. 8m and n). These results indicate that *A. muciniphila* and *Bifidobacterium* are main microflora for enhanced energy expenditure and decreased weight gain on Au@P-NPs treatment in HFD-induced obese animals. This is backed by several earlier investigations revealing that the oral transplantation of *A. muciniphila* to HFD-fed animals inhibited weight gain and related metabolic disorders [61,79,81,82]. But the population size of *A. muciniphila* got elevated at the 3 day PC, as oxygen utilization and body mass alteration become similar between Au@P-NPs-receiver and HFD-receiver animals, indicating that reduced *Lactobacillus* and increased *Bifidobacterium* might play a key role. This is supported by earlier investigations revealing positive correlation between *Lactobacillus* and obesity [3,83], and negative association between *Bifidobacterium* and obesity [84,85]. The remains faecal suspensions from Au@P-NPs-treated

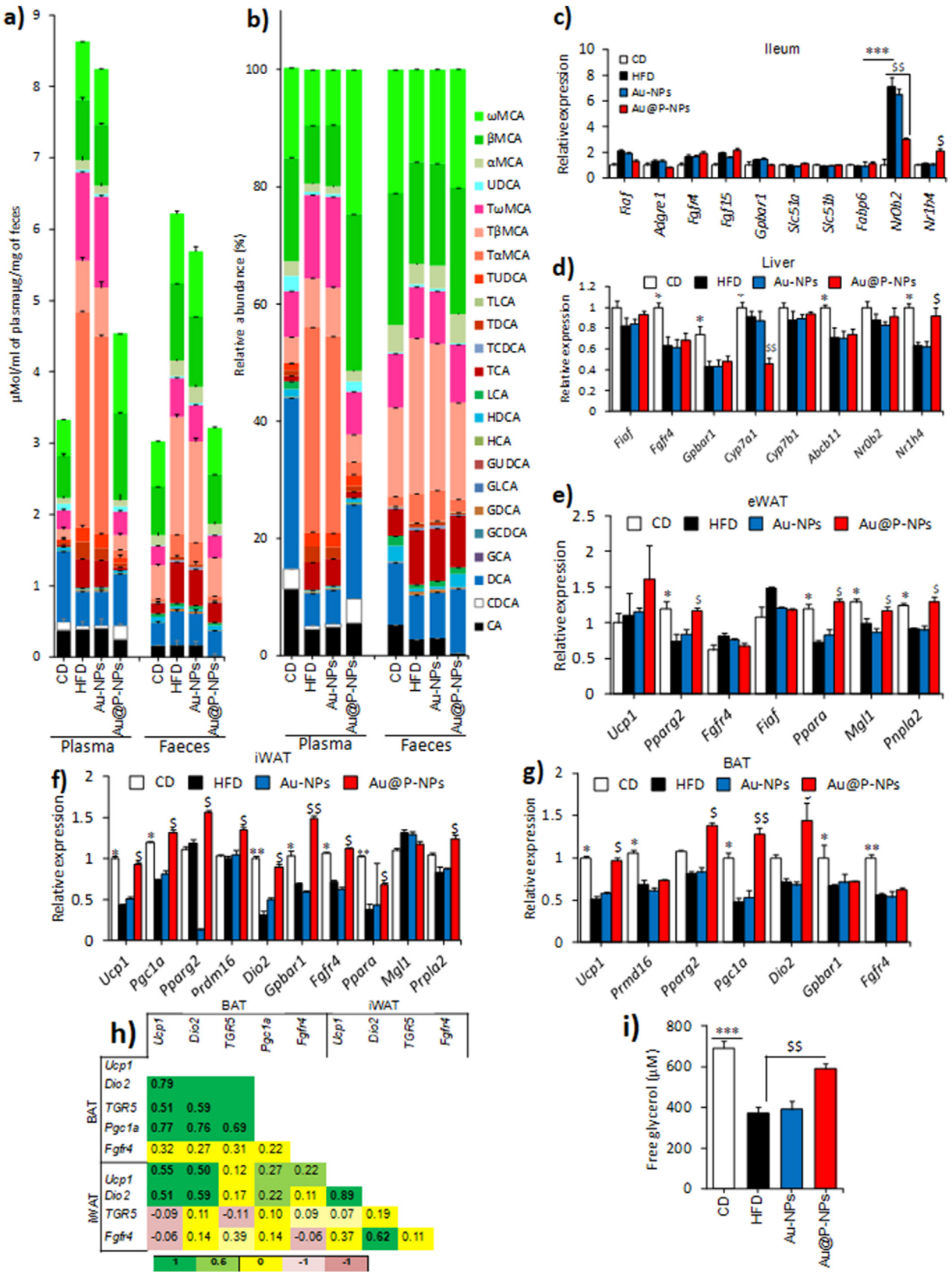

Fig. 7. Changes in bile acid profile of HFD-fed mice after Au@P-NPs. (a) Profile of bile acids in plasma. Profile of bile acids in faecal samples. The mRNA was isolated from indicated fat tissues of mice and the expression pattern of indicated genes was measured by RT-PCR. (c) Ileum. (d) Liver. (e) eWAT. (f) iWAT. (g) BAT. (h) Significant correlation between the mRNA expression profiles of BAT and iWAT (dark values indicate significant levels). (i) Free glycerol content in plasma. One-way ANOVA repeated measurements with BPHT. $^{*}P < 0.05$, $^{**}P < 0.01$ and $^{***}P < 0.001$ for CD *vs* HFD; $^{\$}P < 0.05$, $^{\$\$}P < 0.01$ and $^{\$\$\$}P < 0.001$ for Au@P-NPs *vs* HFD.

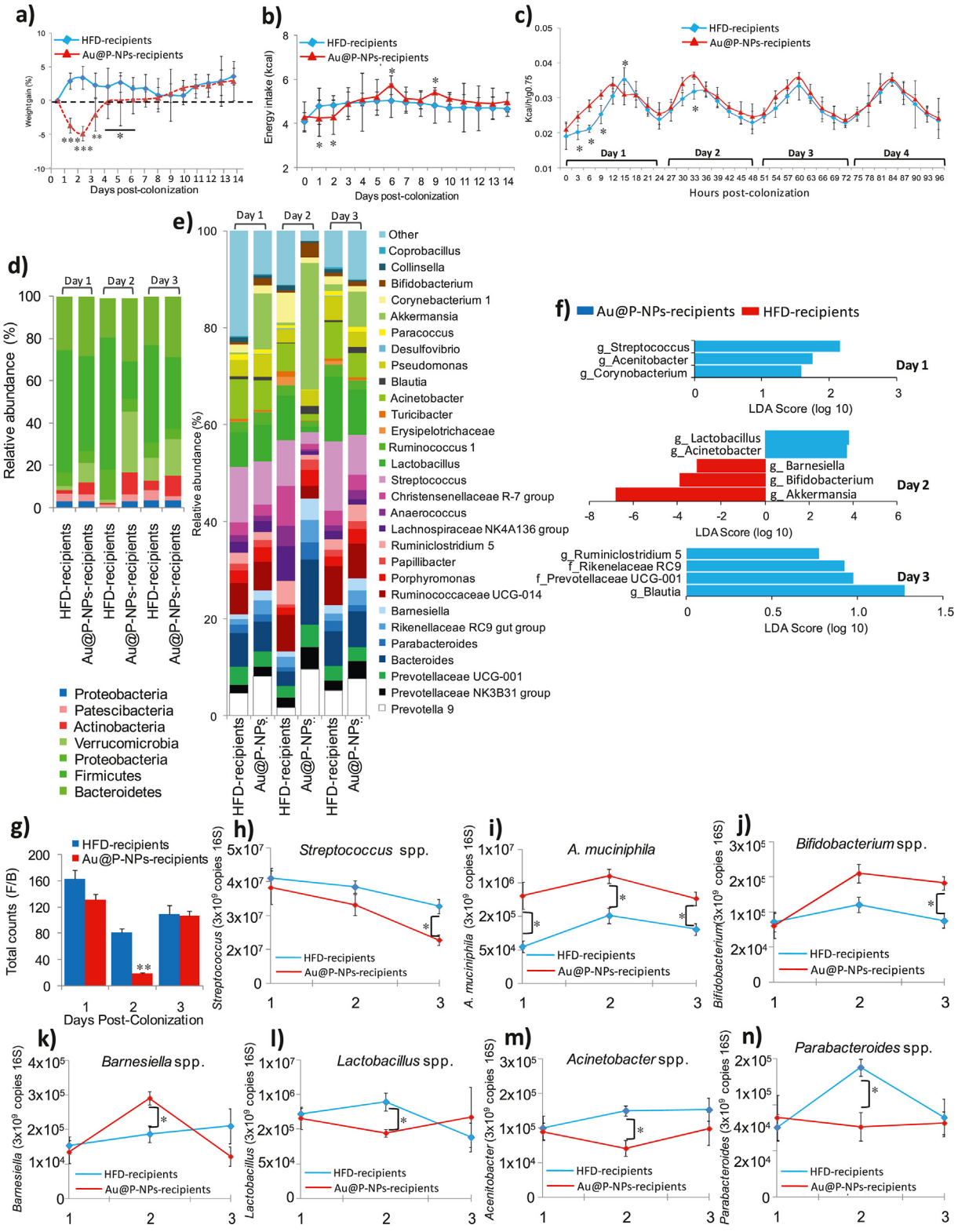

Fig. 8. Re-establishment of germ free (GF) mice with the faecal microbiota of Au@P-NPs-treated animals summarizes the effects of Au@P-NPs on body weight increase and energy expenditure. GF animals were inoculated either with the faecal slurry of HFD-fed animals (HFD recipients) or Au@P-NPs-treated animals (Au@P-NPs recipients) and reserved in metabolic cages with a less-fat containing diet during the early days of PC. Animals were shortly shifted into GF cages and kept under aseptic conditions. (a) body weight increase; (b) energy intake; (c) energy expenditure (the connection among metabolic rate and body weight was stabilized by using body mass$^{0.75}$). (d and e) Taxonomic gut microbial profile of HFD and Au@P-NPs recipients at phylum and the LTL obtained at indicated days PC. (f) LEfSe calculation of taxa at the LTL likely better discriminates the GM of HFD and Au@P-NPs recipients at days PC. (g) F/B ratio in HFD and Au@P-NPs recipients. (g–n) The abundance of specific bacteria was measured by qPCR analysis and the number of copies of each taxon was stabilized by 3×10^9 copies of total bacteria. Two-way frequent measurements ANOVA with BPHT applied to assess the significant differences between time points. $^*P < 0.05$, $^{**}P < 0.01$ and $^{***}P < 0.001$.

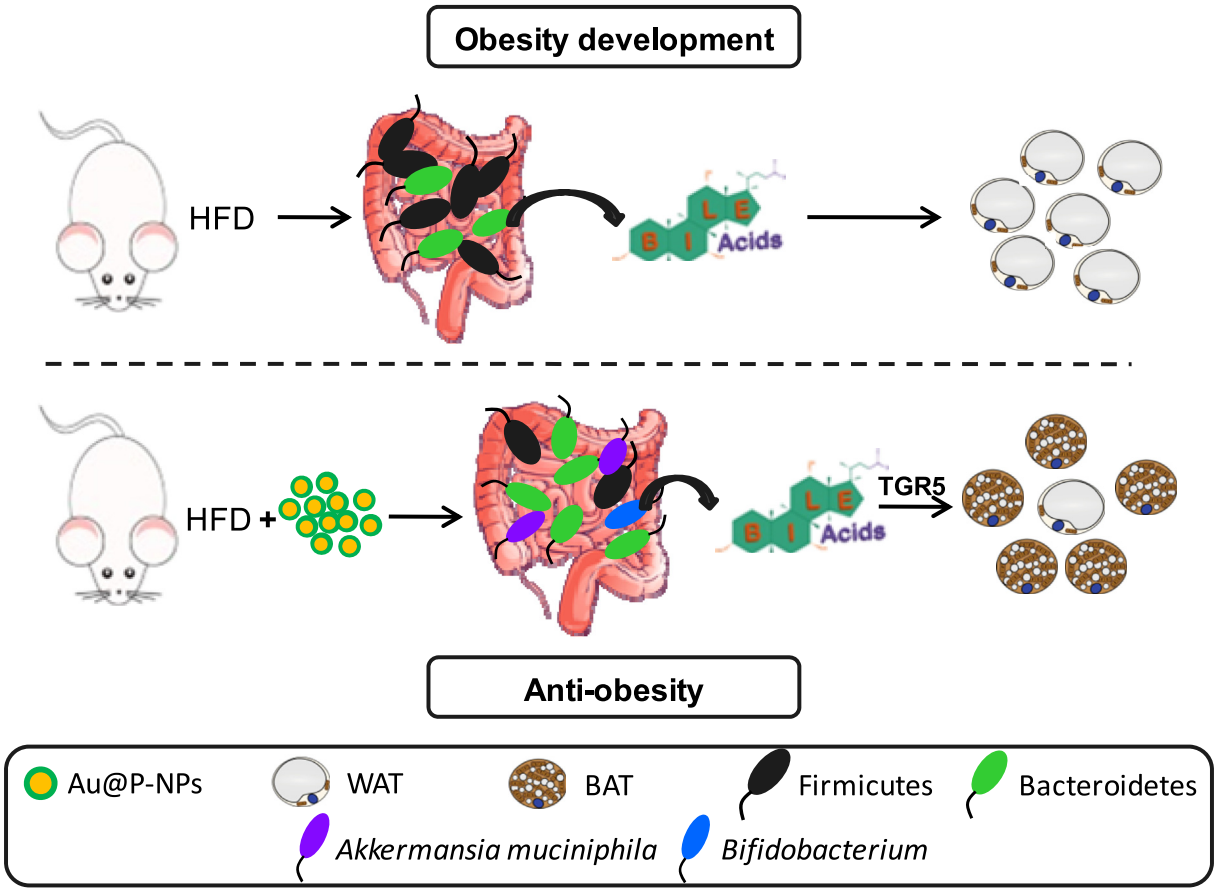

Fig. 9. Mechanism of action of Au@P-NPs for anti-obesity effects. Administration of Au@P-NPs increases energy expenditure and alter bile acid profile through gut microbiota in HFD-induced obese mice to convert WATs into BATs.

and HFD-fed donor animals were combined and total phenolic content (TPC) in these suspensions was quantified [86]. We noticed 0.104 μg gallic acid equivalent (GAE)/mg of faeces in the slurry prepared from Au@P-NPs-treated stools (Fig. S8j). This content is 1099x lower than the TPC noticed in the aqueous extract of *C. verum* bark (AECV; 114.3 μg GAE/mg) (Fig. S8j), suggesting that the gut microbial community of Au@P-NPs recipients were responsible for the anti-obesity effect and not because of the polyphenols present in the faecal resuspensions.

Polyphenols are well known for their potent antioxidant property [87]. The possible increase in the antioxidant effect, as assessed by DPPH (Fig. S9a) and ABTS (Fig. S9b) radical scavenging assays in mice lumen, was related to the phenolic compounds of *C. verum*. Au@P-NPs might decrease the abundance of facultative anaerobes such as Streptococci and Lactobacilli due to hold back oxygen availability. This assumption is supported by a significant decline in the population of *Lactobacillus* species examined in mice administered with the antioxidant tempol and *Myrciaria dubia* [3,75]. Au@P-NPs acted as superior anti-obesity agents as compared to Au-NPs.

4. Conclusion

This study is the first to provide unequivocal evidence that oral administration of *C. verum* derived bioactives-functionalized AuNPs (Au@P-NPs) increases energy expenditure and alters bile acid profile through gut microbiota in HFD-induced obese mice. Au@P-NPs increased mRNA expression of *UCP1* in the brown adipose tissue, altered plasma bile acid profile, and increased the abundance of *A. muciniphila* and *Bifidobacterium* and decreased the abundance of *Lactobacillus* (Fig. 9). FMT revealed lesser weight increase and higher energy expenditure in the GF mice with re-established the gut microbiota through Au@P-NPs treatment compared to GF animals reconstituted with the faecal suspension of HFD-fed mice. Au@P-NPs showed no toxicity sign in liver, lung, kidney, heart, and pancreas, and no significant alteration in blood serum parameters after 8 weeks of administration. Intestinal microbiota reshaping with Au@P-NPs revealed immense potential as alternatives to existing anti-obesity drugs.

Credit author statement

Vivek K. Sharma: Performed experiments, Data analysis & Writing. Prateeksha: Performed experiments, Data analysis & Writing. Sateesh C. Gupta: Performed experiments, Data analysis & Writing. Brahma N. Singh. Conceptualization, Funding, Writing – Review & Editing. Chandana V. Rao: Performed animal experiments, Data analysis & Writing, Ethical Approval. Saroj K. Barik: Conceptualization, Funding, Writing Review & Editing

Declaration of competing interest

The authors declare that they have no known competing financial interests or personal relationships that could have appeared to influence the work reported in this paper.

Acknowledgment

We thank the Council of Science and Industrial Research (CSIR; OLP-0106), India for financial support.

Appendix A. Supplementary data

Supplementary data to this article can be found online at https://doi.org/10.1016/j.mtbio.2022.100204.

References

[1] G.B. Lim, Improved gut microbiota profile in individuals with obesity taking statins, Nat. Rev. Cardiol. 17 (7) (2020), 385-385.

[2] T. Kelly, W. Yang, C.S. Chen, K. Reynolds, J. He, Global burden of obesity in 2005 and projections to 2030, Int. J. Obes. 32 (9) (2008) 1431–1437.

[3] F.F. Anhe, R.T. Nachbar, T.V. Varin, J. Trottier, S. Dudonne, M. Le Barz, P. Feutry, G. Pilon, O. Barbier, Y. Desjardins, D. Roy, A. Marette, Treatment with camu camu (Myrciaria dubia) prevents obesity by altering the gut microbiota and increasing energy expenditure in diet-induced obese mice, Gut 68 (3) (2019) 453–464.

[4] S.J. Olshansky, D.J. Passaro, R.C. Hershow, J. Layden, B.A. Carnes, J. Brody, L. Hayflick, R.N. Butler, D.B. Allison, D.S. Ludwig, A potential decline in life expectancy in the United States in the 21st century, N. Engl. J. Med. 352 (11) (2005) 1138–1145.

[5] L.A. David, C.F. Maurice, R.N. Carmody, D.B. Gootenberg, J.E. Button, B.E. Wolfe, A.V. Ling, A.S. Devlin, Y. Varma, M.A. Fischbach, S.B. Biddinger, R.J. Dutton, P.J. Turnbaugh, Diet rapidly and reproducibly alters the human gut microbiome, Nature 505 (7484) (2014) 559–563.

[6] Y.J. Tak, S.Y. Lee, Anti-Obesity drugs: long-term efficacy and safety: an updated review, World J. Mens Health 39 (2) (2020) 208–221.

[7] S. Vieira-Silva, G. Falony, E. Belda, T. Nielsen, J. Aron-Wisnewsky, R. Chakaroun, S.K. Forslund, K. Assmann, M. Valles-Colomer, T.T.D. Nguyen, S. Proost, E. Prifti, V. Tremaroli, N. Pons, E. Le Chatelier, F. Andreelli, J.P. Bastard, L.P. Coelho, N. Galleron, T.H. Hansen, J.S. Hulot, C. Lewinter, H.K. Pedersen, B. Quinquis, C. Rouault, H. Roume, J.E. Salem, N.B. Sondertoft, S. Touch, C. MetaCardis, M.E. Dumas, S.D. Ehrlich, P. Galan, J.P. Gotze, T. Hansen, J.J. Holst, L. Kober, I. Letunic, J. Nielsen, J.M. Oppert, M. Stumvoll, H. Vestergaard, J.D. Zucker, P. Bork, O. Pedersen, F. Backhed, K. Clement, J. Raes, Statin therapy is associated with lower prevalence of gut microbiota dysbiosis, Nature 581 (7808) (2020) 310–315.

[8] G.B. Lim, Improved gut microbiota profile in individuals with obesity taking statins, Nat. Rev. Cardiol. 17 (7) (2020), 385-385.

[9] E. Le Chatelier, T. Nielsen, J.J. Qin, E. Prifti, F. Hildebrand, G. Falony, M. Almeida, M. Arumugam, J.M. Batto, S. Kennedy, P. Leonard, J.H. Li, K. Burgdorf, N. Grarup, T. Jorgensen, I. Brandslund, H.B. Nielsen, A.S. Juncker, M. Bertalan, F. Levenez, N. Pons, S. Rasmussen, S. Sunagawa, J. Tap, S. Tims, E.G. Zoetendal, S. Brunak, K. Clement, J. Dore, M. Kleerebezem, K. Kristiansen, P. Renault, T. Sicheritz-Ponten, W.M. de Vos, J.D. Zucker, J. Raes, T. Hansen, P. Bork, J. Wang, S.D. Ehrlich, O. Pedersen, M. Consortium, Richness of human gut microbiome correlates with metabolic markers, Nature 500 (7464) (2013) 541–546.

[10] R.X. Liu, J. Hong, X.Q. Xu, Q. Feng, D.Y. Zhang, Y.Y. Gu, J. Shi, S.Q. Zhao, W. Liu, X.K. Wang, H.H. Xia, Z.P. Liu, B. Cui, P.W. Liang, L.Q. Xi, J.B. Jin, X.Y. Ying, X.L. Wang, X.J. Zhao, W.Y. Li, H.J. Jia, Z. Lan, F.Y. Li, R. Wang, Y.K. Sun, M.L. Yang, Y.X. Shen, Z.Y. Jie, J.H. Li, X.M. Chen, H.Z. Zhong, H.L. Xie, Y.F. Zhang, W.Q. Gu, X.X. Deng, B.Y. Shen, X. Xu, H.M. Yang, G.W. Xu, Y.F. Bi, S.H. Lai, J. Wang, L. Qi, L. Madsen, J.Q. Wang, G. Ning, K. Kristiansen, W.Q. Wang, Gut microbiome and serum metabolome alterations in obesity and after weight-loss intervention, Nat. Med. 23 (7) (2017) 859–868.

[11] V.K. Ridaura, J.J. Faith, F.E. Rey, J.Y. Cheng, A.E. Duncan, A.L. Kau, N.W. Griffin, V. Lombard, B. Henrissat, J.R. Bain, M.J. Muehlbauer, O. Ilkayeva, C.F. Semenkovich, K. Funai, D.K. Hayashi, B.J. Lyle, M.C. Martini, L.K. Ursell, J.C. Clemente, W. Van Treuren, W.A. Walters, R. Knight, C.B. Newgard, A.C. Heath, J.I. Gordon, Gut microbiota from twins discordant for obesity modulate metabolism in mice, Science 341 (6150) (2013), 1079-1049.

[12] P.J. Turnbaugh, M. Hamady, T. Yatsunenko, B.L. Cantarel, A. Duncan, R.E. Ley, M.L. Sogin, W.J. Jones, B.A. Roe, J.P. Affourtit, M. Egholm, B. Henrissat, A.C. Heath, R. Knight, J.I. Gordon, A core gut microbiome in obese and lean twins, Nature 457 (7228) (2009) 480–487.

[13] R.E. Ley, P.J. Turnbaugh, S. Klein, J.I. Gordon, Microbial ecology - human gut microbes associated with obesity, Nature 444 (7122) (2006) 1022–1023.

[14] P.J. Turnbaugh, F. Baeckhed, L. Fulton, J.I. Gordon, Diet-induced obesity is linked to marked but reversible alterations in the mouse distal gut microbiome, Cell Host Microbe 3 (4) (2008) 213–223.

[15] F. Backhed, J.K. Manchester, C.F. Semenkovich, J.I. Gordon, Mechanisms underlying the resistance to diet-induced obesity in germ-free mice, Proc. Natl. Acad. Sci. USA 104 (3) (2007) 979–984.

[16] J.K. Hodges, J. Zhu, Z. Yu, Y. Vodovotz, G. Brock, G.Y. Sasaki, P. Dey, R.S. Bruno, Intestinal-level anti-inflammatory bioactivities of catechin-rich green tea: rationale, design, and methods of a double-blind, randomized, placebo-controlled crossover trial in metabolic syndrome and healthy adults, Contemp. Clin. Trials Commun. 17 (2020), 100495.

[17] M.L. Jones, C. Tomaro-Duchesneau, S. Prakash, The gut microbiome, probiotics, bile acids axis, and human health, Trends Microbiol. 22 (6) (2014) 306–308.

[18] M. Watanabe, S.M. Houten, C. Mataki, M.A. Christoffolete, B.W. Kim, H. Sato, N. Messaddeq, J.W. Harney, O. Ezaki, T. Kodama, K. Schoonjans, A.C. Bianco, J. Auwerx, Bile acids induce energy expenditure by promoting intracellular thyroid hormone activation, Nature 439 (7075) (2006) 484–489.

[19] D.P. Singh, P. Khare, V. Bijalwan, R.K. Baboota, J. Singh, K.K. Kondepudi, K. Chopra, M. Bishnoi, Coadministration of isomalto-oligosaccharides augments metabolic health benefits of cinnamaldehyde in high fat diet fed mice, Biofactors 43 (6) (2017) 821–835.

[20] P. Khare, S. Jagtap, Y. Jain, R.K. Baboota, P. Mangal, R.K. Boparai, K.K. Bhutani, S.S. Sharma, L.S. Premkumar, K.K. Kondepudi, K. Chopra, M. Bishnoi, Cinnamaldehyde supplementation prevents fasting-induced hyperphagia, lipid accumulation, and inflammation in high-fat diet-fed mice, Biofactors 42 (2) (2016) 201–211.

[21] B.N. Singh, Prateeksha, G. Pandey, V. Jadaun, S. Singh, R. Bajpai, S. Nayaka, A.H. Naqvi, A.K.S. Rawat, D.K. Upreti, B.R. Singh, Development and characterization of a novel Swarna-based herbo-metallic colloidal nano-formulation - inhibitor of Streptococcus mutans quorum sensing, RSC Adv. 5 (8) (2015) 5809–5822.

[22] A. Kumar Singh, C. Cabral, R. Kumar, R. Ganguly, H. Kumar Rana, A. Gupta, M. Rosaria Lauro, C. Carbone, F. Reis, A.K. Pandey, Beneficial effects of dietary polyphenols on gut microbiota and strategies to improve delivery efficiency, Nutrients 11 (9) (2019) 2216.

[23] D. Pal, C.K. Sahu, A. Haldar, Bhasma : the ancient Indian nanomedicine, J. Adv. Pharm. Technol. Res. (JAPTR) 5 (1) (2014) 4–12.

[24] Brooks RAWaRR, Gold and silver in medicine, in: Noble Metals and Biological Systems, CRC Press, 1992, pp. 277–279.

[25] H. Gopinath, M. Shivashankar, Herbo-metallic Indian nano-medicine Abhrak Bhasma (MICA): a periodical review, Res. J. Pharmaceut. Biol. Chem. Sci. 7 (2016) 2373–2381.

[26] J. Liu, F. Zhang, V. Ravikanth, O.A. Olajide, C. Li, L.-X. Wei, Chemical compositions of metals in bhasmas and Tibetan Zuotai are a major determinant of their therapeutic effects and toxicity, Evid-Based Compl. Alt. 2019 (2019), 1697804.

[27] P. Prateeksha, R. Bajpai, C.V. Rao, D.K. Upreti, S.K. Barik, B.N. Singh, Chrysophanol-functionalized silver nanoparticles for anti-adhesive and anti-biofouling coatings to prevent urinary catheter-associated infections, ACS Appl. Nano Mater. 4 (2) (2021) 1512–1528.

[28] Rao CV. Prateeksha, A.K. Das, S.K. Barik, B.N. Singh, ZnO/curcumin nanocomposites for enhanced inhibition of Pseudomonas aeruginosa virulence via LasR-RhlR quorum sensing systems, Mol. Pharm. 16 (8) (2019) 3399–3413.

[29] Barik SK. Prateeksha, B.N. Singh, Nanoemulsion-loaded hydrogel coatings for inhibition of bacterial virulence and biofilm formation on solid surfaces, Sci. Rep. 9 (2019) 6520.

[30] Prateeksha, B.R. Singh, V.K. Gupta, F. Deeba, R. Bajpai, V. Pandey, A.H. Naqvi, D.K. Upreti, N. Gathergood, Y.M. Jiang, H.A. El Enshasy, E.N. Sholkamy, A.A. Mostafa, A. Hesham, B.N. Singh, Non-toxic and ultra-small biosilver nanoclusters trigger apoptotic cell death in fluconazole-resistant Candida albicans via Ras signaling, Biomolecules 9 (2) (2019) 47.

[31] B.N. Singh, B.R. Singh, V.K. Gupta, R.N. Kharwar, L. Pecoraro, Coating with microbial hydrophobins: a novel approach to develop smart drug nanoparticles, Trends Biotechnol. 36 (11) (2018) 1103–1106.

[32] Prateeksha, B.R. Singh, M. Shoeb, S. Sharma, A.H. Naqvi, V.K. Gupta, B.N. Singh, Scaffold of selenium nanovectors and honey phytochemicals for inhibition of Pseudomonas aeruginosa quorum sensing and biofilm formation, Front. Cell Infect. Microbiol. 7 (2017) 93.

[33] B.R. Singh, B.N. Singh, A. Singh, W. Khan, A.H. Naqvi, H.B. Singh, Mycofabricated biosilver nanoparticles interrupt Pseudomonas aeruginosa quorum sensing systems, Sci. Rep. 5 (2015) 13719.

[34] B.N. Singh, A.K.S. Rawat, W. Khan, A.H. Naqvi, B.R. Singh, Biosynthesis of stable antioxidant zno nanoparticles by Pseudomonas aeruginosa rhamnolipids, PLoS One 9 (9) (2014), 106937.

[35] S. Simu, A. Sungeun, V. Castro-Aceituno, P. Singh, R. Mathiyalagan, Z. Jimenez, J. Hurh, Y.-J. Kim, D.-C. Yang, Gold nanoparticles synthesized with fresh Panax ginseng Leaf extract suppress adipogenesis by downregulating PPARγ/CEBPα signaling in 3T3-L1 mature adipocytes, J. Nanosci. Nanotechnol. 19 (2) (2018) 701–708.

[36] S.C. Hui, Y. Liu, L. Huang, L. Zheng, M. Zhou, H.D. Lang, X.L. Wang, L. Yi, M.T. Mi, Resveratrol enhances brown adipose tissue activity and white adipose tissue browning in part by regulating bile acid metabolism via gut microbiota remodeling, Int. J. Obes. 44 (8) (2020) 1678–1690.

[37] P. Wang, D.T. Li, W.X. Ke, D. Liang, X.S. Hu, F. Chen, Resveratrol-induced gut microbiota reduces obesity in high-fat diet-fed mice, Int. J. Obes. 44 (1) (2020) 213–225.

[38] X. Han, J. Guo, Y. You, J. Zhan, W. Huang, p-Coumaric acid prevents obesity via activating thermogenesis in brown adipose tissue mediated by mTORC1-RPS6, Faseb. J. 34 (6) (2020) 7810–7824.

[39] J. Choi, S. Oh, M. Son, K. Byun, Pyrogallol-phloroglucinol-6,6-bieckol alleviates obesity and systemic inflammation in a mouse model by reducing expression of RAGE and RAGE ligands, Mar. Drugs 17 (11) (2019) 612.

[40] J. Jiang, M.P. Emont, H. Jun, X. Qiao, J. Liao, D.I. Kim, J. Wu, Cinnamaldehyde induces fat cell-autonomous thermogenesis and metabolic reprogramming, Metab. Clin. Exp. 77 (2017) 58–64.

[41] W.W. Wang, Y. Pan, H. Zhou, L. Wang, X. Chen, G. Song, J.X. Liu, A.K. Li, Ferulic acid suppresses obesity and obesity-related metabolic syndromes in high fat diet-induced obese C57BL/6J mice, Food Agric. Immunol. 29 (1) (2018) 1116–1125.

[42] M.N. Chen, C.F. Chan, S.L. Huang, Y.S. Lin, Green biosynthesis of gold nanoparticles using Chenopodium formosanum shell extract and analysis of the particles' antibacterial properties, J. Sci. Food Agric. 99 (7) (2019) 3693–3702.

[43] N. Seurre, J. Sepioł, F. Lahmani, A. Zehnacker-Rentien, K. Le Barbu-Debus, Vibrational study of the S0 and S1 states of 2-naphthyl-1-ethanol/(water)2 and 2-naphthyl-1-ethanol/(methanol)2 complexes by IR/UV double resonance spectroscopy, Phys. Chem. Chem. Phys. 6 (19) (2004) 4658–4664.

[44] R. Majumdar, B.G. Bag, N. Maity, Acacia nilotica (Babool) leaf extract mediated size-controlled rapid synthesis of gold nanoparticles and study of its catalytic activity, Int. Nano Lett. 3 (2013) 53.
[45] N.K.R. Bogireddy, U. Pal, L.M. Gomez, V. Agarwal, Size controlled green synthesis of gold nanoparticles using Coffea arabica seed extract and their catalytic performance in 4-nitrophenol reduction, RSC Adv. 8 (44) (2018) 24819–24826.
[46] J. D'Angelo, FT-IR determination of aliphatic and aromatic C-H contents of fossil leaf compressions. Part 2: applications, Anu. Latinoam. (Lublin, Internet) 18 (2004) 34–38.
[47] P. Singh, Y.J. Kim, D.B. Zhang, D.C. Yang, Biological synthesis of nanoparticles from plants and microorganisms, Trends Biotechnol. 34 (7) (2016) 588–599.
[48] C.H. Lai, C.Y. Lin, H.T. Wu, H.S. Chan, Y.J. Chuang, C.T. Chen, C.C. Lin, Galactose encapsulated multifunctional nanoparticle for HepG2 cell internalization, Adv. Funct. Mater. 20 (22) (2010) 3948–3958.
[49] C.D. Raposo, C.A. Conceicao, M.T. Barros, Nanoparticles based on novel carbohydrate-functionalized polymers, Molecules 25 (7) (2020).
[50] B.V. Ramana, V.V. Kumar, P.N.R. Krishna, C.S. Kumar, P.U.M. Reddy, T.N. Raju, Effect of quercetin on galactose-induced hyperglycaemic oxidative stress in hepatic and neuronal tissues of Wistar rats, Acta Diabetol. 43 (4) (2006) 135–141.
[51] J. Choi, S. Oh, M. Son, K. Byun, Pyrogallol-phloroglucinol-6,6-bieckol alleviates obesity and systemic inflammation in a mouse model by reducing expression of RAGE and RAGE ligands, Mar. Drugs 17 (11) (2019) 612.
[52] J. Jiang, M.P. Emont, H. Jun, X. Qiao, J. Liao, D-i Kim, J. Wu, Cinnamaldehyde induces fat cell-autonomous thermogenesis and metabolic reprogramming, Metabolism 77 (2017) 58–64.
[53] W. Wang, Y. Pan, H. Zhou, L. Wang, X. Chen, G. Song, J. Liu, A. Li, Ferulic acid suppresses obesity and obesity-related metabolic syndromes in high fat diet-induced obese C57BL/6J mice, Food Agric. Immunol. 29 (1) (2018) 1116–1125.
[54] K. Mnafgui, A. Derbali, S. Sayadi, N. Gharsallah, A. Elfeki, N. Allouche, Anti-obesity and cardioprotective effects of cinnamic acid in high fat diet- induced obese rats, J. Food Sci. Technol. 52 (7) (2015) 4369–4377.
[55] S. Sudheer, P. Gangwar, Z. Usmani, M. Sharma, V.K. Sharma, S.S. Sana, F. Almeida, N.K. Dubey, D.P. Singh, N. Dilbaghi, H.R. Khayat Kashani, V.K. Gupta, B.N. Singh, M. Khayatkashani, S.M. Nabavi, Shaping the gut microbiota by bioactive phytochemicals: an emerging approach for the prevention and treatment of human diseases, Biochimie (21) (2021) 247–249. S0300-9084.
[56] Y.T. Tung, M.T. Chua, S.Y. Wang, S.T. Chang, Anti-inflammation activities of essential oil and its constituents from indigenous cinnamon (Cinnamomum osmophloeum) twigs, Bioresour. Technol. 99 (9) (2008) 3908–3913.
[57] L.D. Fideles, J.A.L. de Miranda, C.D. Martins, M.L.L. Barbosa, H.B. Pimenta, P.V.D. Pimentel, C.S. Teixeira, M.A.S. Scafuri, S.D. Facanha, J.E.F. Barreto, P.M.D. Carvalho, A.G. Scafuri, J.L. Araujo, J.A. Rocha, I.G.P. Vieira, N.M.P.S. Ricardo, M.D. Campelo, M.E.N.P. Ribeiro, G.A.D. Brito, G.S. Cerqueira, Role of rutin in 5-fluorouracil-induced intestinal mucositis: prevention of histological damage and reduction of inflammation and oxidative stress, Molecules 25 (12) (2020) 2786.
[58] T. McLaughlin, A. Deng, G. Yee, C. Lamendola, G. Reaven, P.S. Tsao, S.W. Cushman, A. Sherman, Inflammation in subcutaneous adipose tissue: relationship to adipose cell size, Diabetologia 53 (2) (2010) 369–377.
[59] J. Miyamoto, M. Igarashi, K. Watanabe, S-i Karaki, H. Mukouyama, S. Kishino, X. Li, A. Ichimura, J. Irie, Y. Sugimoto, T. Mizutani, T. Sugawara, T. Miki, J. Ogawa, D.J. Drucker, M. Arita, H. Itoh, I. Kimura, Gut microbiota confers host resistance to obesity by metabolizing dietary polyunsaturated fatty acids, Nat. Commun. 10 (1) (2019) 4007.
[60] A. Cotillard, S.P. Kennedy, L.C. Kong, E. Prifti, N. Pons, E. Le Chatelier, M. Almeida, B. Quinquis, F. Levenez, N. Galleron, S. Gougis, S. Rizkalla, J.M. Batto, P. Renault, J. Dore, J.D. Zucker, K. Clement, S.D. Ehrlich, A.M. Consortium, Dietary intervention impact on gut microbial gene richness, Nature 500 (7464) (2013) 585–588.
[61] H. Plovier, A. Everard, C. Druart, C. Depommier, M. Van Hul, L. Geurts, J. Chilloux, N. Ottman, T. Duparc, L. Lichtenstein, A. Myridakis, N.M. Delzenne, J. Klievink, A. Bhattacharjee, K.C.H. van der Ark, S. Aalvink, L.O. Martinez, M.E. Dumas, D. Maiter, A. Loumaye, M.P. Hermans, J.P. Thissen, C. Belzer, W.M. de Vos, P.D. Cani, A purified membrane protein from Akkermansia muciniphila or the pasteurized bacterium improves metabolism in obese and diabetic mice, Nat. Med. 23 (1) (2017) 107–113.
[62] D.A. Russell, R.P. Ross, G.F. Fitzgerald, C. Stanton, Metabolic activities and probiotic potential of bifidobacteria, Int. J. Food Microbiol. 149 (1) (2011) 88–105.
[63] Q.Y. Lu, A.M. Rasmussen, J.P. Yang, R.P. Lee, J.J. Huang, P. Shao, C.L. Carpenter, I. Gilbuena, G. Thames, S.M. Henning, D. Heber, Z.P. Li, Mixed spices at culinary doses have prebiotic effects in healthy adults: a pilot study, Nutrients 11 (6) (2019) 1425.
[64] F.H. Guo, H. Xiong, X.Y. Wang, L. Jiang, N.X. Yu, Z.Y. Hu, Y. Sun, R. Tsao, Phenolics of green pea (Pisum sativum L.) Hulls, their plasma and urinary metabolites, bioavailability, and in vivo antioxidant activities in a rat model, J. Agric. Food Chem. 67 (43) (2019) 11955–11968.
[65] S.M. Henning, P.H. Summanen, R.P. Lee, J.P. Yang, S.M. Finegold, D. Heber, Z.P. Li, Pomegranate ellagitannins stimulate the growth of Akkermansia muciniphila in vivo, Anaerobe 43 (2017) 56–60.
[66] Y.C. Zanzer, M. Plaza, A. Dougkas, C. Turner, I. Bjorck, E. Ostman, Polyphenol-rich spice-based beverages modulated postprandial early glycaemia, appetite and PYY after breakfast challenge in healthy subjects: a randomized, single blind, crossover study, J. Funct.Foods 35 (2017) 574–583.
[67] L.L. Qi, H.G. Mao, X.H. Lu, T.T. Shi, J.B. Wang, Cinnamaldehyde promotes the intestinal barrier functions and reshapes gut microbiome in early weaned rats, Front Nutr. 8 (2021), 748503.
[68] X.L. Guo, R.Y. Tang, S.Y. Yang, Y.R. Lu, J. Luo, Z.H. Liu, Rutin and its combination with inulin attenuate gut dysbiosis, the inflammatory status and endoplasmic reticulum stress in paneth cells of obese mice induced by high-fat diet, Front. Microbiol. 9 (2018) 2651.
[69] T.T. Guo, D. Song, L. Cheng, X. Zhang, Interactions of tea catechins with intestinal microbiota and their implication for human health, Food Sci. Biotechnol. 28 (6) (2019) 1617–1625.
[70] R. Santangelo, A. Silvestrini, C. Mancuso, Ginsenosides, catechins, quercetin and gut microbiota: current evidence of challenging interactions, Food Chem. Toxicol. 123 (2019) 42–49.
[71] H. Taoka, Y. Yokoyama, K. Morimoto, N. Kitamura, T. Tanigaki, Y. Takashina, K. Tsubota, M. Watanabe, Role of bile acids in the regulation of the metabolic pathways, World J. Diabetes 7 (13) (2016) 260–270.
[72] S. Devkota, Y.W. Wang, M.W. Musch, V. Leone, H. Fehlner-Peach, A. Nadimpalli, D.A. Antonopoulos, B. Jabri, E.B. Chang, Dietary-fat-induced taurocholic acid promotes pathobiont expansion and colitis in Il10(-/-) mice, Nature 487 (7405) (2012) 104–+.
[73] B. Goodwin, S.A. Jones, R.R. Price, M.A. Watson, D.D. McKee, L.B. Moore, C. Galardi, J.G. Wilson, M.C. Lewis, M.E. Roth, P.R. Maloney, T.M. Willson, S.A. Kliewer, A regulatory cascade of the nuclear receptors FXR, SHP-1, and LRH-1 represses bile acid biosynthesis, Mol. Cell. 6 (3) (2000) 517–526.
[74] K.Z. Jia, D.P. Zhang, Q. Jia, Q.Y. Zhang, Regulation of Fgf15 expression in the intestine by glucocorticoid receptor, Mol. Med. Rep. 19 (4) (2019) 2953–2959.
[75] F. Li, C.T. Jiang, K.W. Krausz, Y.F. Li, I. Albert, H.P. Hao, K.M. Fabre, J.B. Mitchell, A.D. Patterson, F.J. Gonzalez, Microbiome remodelling leads to inhibition of intestinal farnesoid X receptor signalling and decreased obesity, Nat. Commun. 4 (2013) 2384.
[76] M. Watanabe, Y. Horai, S.M. Houten, K. Morimoto, T. Sugizaki, E. Arita, C. Mataki, H. Sato, Y. Tanigawara, K. Schoonjans, H. Itoh, J. Auwerx, Lowering bile acid pool size with a synthetic farnesoid X receptor (FXR) agonist induces obesity and diabetes through reduced energy expenditure, J. Biol. Chem. 286 (30) (2011) 26913–26920.
[77] S. Fang, J.M. Suh, S.M. Reilly, E. Yu, O. Osborn, D. Lackey, E. Yoshihara, A. Perino, S. Jacinto, Y. Lukasheva, A.R. Atkins, A. Khvat, B. Schnab, R.T. Yu, D.A. Brenner, S. Coulter, C. Liddle, K. Schoonjans, J.M. Olefsky, A.R. Saltiel, M. Downes, R.M. Evans, Intestinal FXR agonism promotes adipose tissue browning and reduces obesity and insulin resistance, Nat. Med. 21 (2) (2015) 159–165.
[78] F.F. Anhe, T.V. Varin, M. Le Barz, Y. Desjardins, E. Levy, D. Roy, A. Marette, Gut microbiota dysbiosis in obesity-linked metabolic diseases and prebiotic potential of polyphenol-rich extracts, Curr. Obes. Rep. 4 (4) (2015) 389–400.
[79] F.F. Anhe, A. Marette, A microbial protein that alleviates metabolic syndrome, Nat. Med. 23 (1) (2017) 11–12.
[80] S. Spring, B. Bunk, C. Sproer, P. Schumann, M. Rohde, B.J. Tindall, H.P. Klenk, Characterization of the first cultured representative of Verrucomicrobia subdivision 5 indicates the proposal of a novel phylum, ISME J. 10 (12) (2016) 2801–2816.
[81] A. Everard, C. Belzer, L. Geurts, J.P. Ouwerkerk, C. Druart, L.B. Bindels, Y. Guiot, M. Derrien, G.G. Muccioli, N.M. Delzenne, W.M. de Vos, P.D. Cani, Cross-talk between Akkermansia muciniphila and intestinal epithelium controls diet-induced obesity, Proc. Natl. Acad. Sci. USA 110 (22) (2013) 9066.
[82] Z. Li, H. Jin, S.Y. Oh, G.E. Ji, Anti-obese effects of two Lactobacilli and two Bifidobacteria on ICR mice fed on a high fat diet, Biochem. Bioph. Res. Co 480 (2) (2016) 222–227.
[83] F. Armougom, M. Henry, B. Vialettes, D. Raccah, D. Raoult, Monitoring bacterial community of human gut microbiota reveals an increase in Lactobacillus in obese patients and methanogens in anorexic patients, PLoS One 4 (9) (2009), e7125.
[84] M. Million, M. Maraninchi, M. Henry, F. Armougom, H. Richet, P. Carrieri, R. Valero, D. Raccah, B. Vialettes, D. Raoult, Obesity-associated gut microbiota is enriched in Lactobacillus reuteri and depleted in Bifidobacterium animalis and Methanobrevibacter smithii, Int. J. Obes. 36 (6) (2012) 817–825.
[85] H.M. An, S.Y. Park, D.K. Lee, J.R. Kim, M.K. Cha, S.W. Lee, H.T. Lim, K.J. Kim, N.J. Ha, Antiobesity and lipid-lowering effects of Bifidobacterium spp. in high fat diet-induced obese rats, Lipids Health Dis. 10 (2011).
[86] H.B. Singh, B.N. Singh, S.P. Singh, C.S. Nautiyal, Solid-state cultivation of Trichoderma harzianum NBRI-1055 for modulating natural antioxidants in soybean seed matrix, Bioresour. Technol. 101 (16) (2010) 6444–6453.
[87] I. Gulcin, R. Kaya, A.C. Goren, H. Akincioglu, M. Topal, Z. Bingol, K. Cetin Çakmak, S.B. Ozturk Sarikaya, L. Durmaz, S. Alwasel, Anticholinergic, antidiabetic and antioxidant activities of cinnamon (cinnamomum verum) bark extracts: polyphenol contents analysis by LC-MS/MS, Int. J. Food Prop. 22 (1) (2019) 1511–1526.